Construction and Building Materials 444 (2024) 137845

Contents lists available at ScienceDirect

Construction and Building Materials

journal homepage: www.elsevier.com/locate/conbuildmat

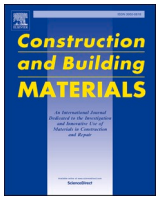

Synergistic effects of fiber hybridization on the fracture toughness of seawater sea-sand concrete

Amirhesam Mashayekhi [a], Reza Hassanli [a,*], Yan Zhuge [a], Xing Ma [a], Christopher W.K. Chow [a], Milad Bazli [b], Allan Manalo [c]

[a] Sustainable Infrastructure and Resource Management (SIRM), UniSA STEM, University of South Australia, Mawson Lakes, SA 5095, Australia
[b] Faculty of Science and Technology, Charles Darwin University, Darwin 0810, Australia
[c] Center for Future Materials, School of Engineering, University of Southern Queensland, QLD 4350, Australia

ARTICLE INFO

Keywords:
Fiber-reinforced concrete
Seawater
Sea-sand
Fracture toughness
Hybrid fiber
Synergy

ABSTRACT

This study investigates the fracture behavior of fiber-reinforced seawater sea-sand concrete (FR-SWSSC), focusing on the impact of fiber hybridization on fracture toughness properties and potential synergistic effects. The study employed micro-fibers including short polypropylene (PPS), polyvinyl alcohol (PVA), basalt fibers (BF), and macro-fibers consisting long polypropylene (PPL) and twisted polypropylene (TPPL) fibers. The results indicated that macro-fibers, PPL and TPPL, significantly enhanced the post-peak behavior of SWSSC, increasing fracture energy by 144 % and 93 % respectively, while micro-fibers alone showed negligible impact on the post-peak behavior. Micro-fiber hybridization significantly enhanced both flexural strength and fracture energy of SWSSC, with hybrid PPS/BF and PPS/PVA demonstrated notably improved fracture energy by 176 % and 290 %, respectively, compared to mono PPS. Hybrid combinations of micro/macro-fibers demonstrated a synergistic effect on fracture toughness, where PPL and TPPL fibers bridged larger cracks, activating micro-fibers for enhanced energy dissipation. Moreover, the strong interfacial bond of PVA and BF fibers with the concrete matrix improved macro-fiber bonding strength and overall fracture resistance. By exploring the synergistic effect of hybrid discrete fibers in enhancing the fracture performance of FR-SWSSC, this research promotes sustainable construction practices by addressing inherent challenges of SWSSC.

1. Introduction

Concrete production significantly impacts the environment due to high water consumption and river sand/gravel extraction [1,2]. This is particularly concerning with the looming global water crisis, with predictions of water scarcity for over half the population by 2050 [3]. River sand extraction further exacerbates ecological disruption in river ecosystems. Additionally, cement production, a key component of concrete, generates significant CO_2 emissions, which reached to 2.8 billion tons in 2019 [4]. Consequently, research prioritizes identifying more sustainable concrete materials to reduce greenhouse gas emissions [5–7]. Seawater (SW) and sea-sand (SS) emerge as promising replacements for freshwater (FW) and normal river sand (NS) due to their abundance and ease of extraction and transport, particularly in coastal projects and remote areas with limited access to high-quality materials due to scarcity or transportation costs [2, 8–10]. The utilization of seawater sea-sand concrete (SWSSC) presents a promising approach for sustainable construction, particularly for coastal structures. However, to ensure its successful implementation as a viable alternative, a thorough understanding of its properties is crucial.

The presence of various ions in SWSSC, including sodium (Na^+), potassium (K^+), chloride (Cl^-), sulphate (SO_4^{2-}), calcium (Ca^{2+}), and magnesium (Mg^{2+}), can impact the properties of both fresh and hardened SWSSC compared to freshwater normal sand concrete (FWNSC). The presence of chloride in SW and SS accelerates cement hydration [11, 12], resulting in higher compressive strength at an early age of SWSSC [12–17]. Furthermore, most studies have shown that the tensile and flexural strength of SWSSC is lower than FWNSC [12, 13, 18, 19]. Additionally, the use of SW and SS, containing chloride ions, can lead to carbonation of the concrete and corrosion of steel in steel reinforced concrete structures, negatively impacting their long-term performance [2, 20]. To improve the durability of SWSS-RC structures, it is crucial to enhance crack resistance and understand the fracture behavior of SWSSC.

Previous studies employed fibers (natural or synthetic) to improve

* Corresponding author.

https://doi.org/10.1016/j.conbuildmat.2024.137845
Received 13 June 2024; Received in revised form 26 July 2024; Accepted 6 August 2024
Available online 11 August 2024

the crack resistance of both SWSSC and FWNSC, leading to improve long-term performance [17, 21–23]. Fiber-reinforced concrete (FRC) exhibited improved energy absorption and ductility compared to normal concrete [24–27]. Synthetic fibers (e.g. polypropylene (PP) and polyvinyl alcohol (PVA)) are popular FRC choices due to their affordability, positive influence on concrete properties, and environmental resilience [17, 28, 29]. Studies showed that the mechanical bonding between PP fibers and concrete resulted in fiber pull-out, whereas PVA fibers exhibited rupture due to their chemical bond with the concrete matrix [30]. Research on FRC using micro-PP and PVA fibers in SWSSC demonstrated significant improvements in flexural strength, fracture energy, and post-peak behavior [30]. Both PP and PVA fiber inclusion transformed SWSSC failure mode from brittle to ductile under compression [17, 31]. Incorporation of PP and PVA fibers also increased splitting tensile strength by 17 % and 23 % compared to plain SWSSC [17]. Incorporation of basalt fiber (BF) into SWSSC demonstrated that a fiber length of 12 mm and a volume fraction of 0.6 % constitute optimal parameters. Under these conditions, compressive strength increased by 9 % and splitting tensile strength by 7 % compared to control specimens [32].

Fiber incorporation improves SWSSC strength and ductility, but the impact of hybrid fibers, particularly on flexural and fracture behavior, remains unexamined. While mono-fibers reinforce concrete, their limitations—length, tensile strength, and bonding strength— in crack control of concrete are well-documented [31, 33, 34]. A meticulously designed hybrid fiber system, combining micro and macro-fibers based on specific properties, has the potential to overcome these limitations and enhance the overall mechanical performance, ductility, and durability of FWNSC [35–41]. Hybrid fiber-reinforced concrete (HFRC) offers superior strength, ductility, toughness, and energy absorption [29, 42–44]. In HFRC, higher-modulus fibers enhance strength, while lower-modulus fibers improve ductility [45]. Studies demonstrate the synergistic effect of fiber hybridization in SWSSC. PVA-basalt fiber (BF) hybridization significantly improved total energy absorption and residual compressive strength compared to mono-BF at the same fiber content (44 % and 181 % increase, respectively) [31]. Similarly, PVA-long PP (PPL) hybridization exhibited substantially higher ductility and residual compressive strength (59 % and 65 % increase, respectively) compared to mono-PPL [31]. Furthermore, adding 3 % macro-BF significantly increased ultra-high performance (UHP) SWSSC compressive strength by 26 %, while micro-PP and BF additions maintained compressive strength [33]. Hybridization of micro-BF/PP fibers in SWSS mortars demonstrated the potential to enhance flexural, compressive, direct tensile, and splitting tensile strengths compared to incorporating mono-fibers. Optimal results were observed with a fiber dosage of 0.4 % for each fiber type in the hybrid system [46].

Fiber-reinforced SWSSC (FR-SWSSC), a relatively new sustainable construction material, requires further investigation to understand its properties and industrial applications. Existing research on its mechanical properties (splitting tensile strength, elastic modulus, compressive strength, etc.) is limited and mostly focused on single fiber types [17, 21, 30, 31, 33]. SWSSC exhibits distinct physical and chemical properties compared to conventional concrete. This substantial chemical reactivity in SWSSC can potentially influence fiber synergies and interfacial bonding, both of which are critical for the performance of hybrid fiber mixes. Additionally, fracture toughness, a crucial property of concrete that reveals crack resistance and propagation, ductility, and post-crack behavior, all of which are valuable for both design optimization and durability assessment of concrete structures, needs thorough evaluation for FR-SWSSC as well. This study comprehensively investigates the potential effects of hybrid fibers on the fracture toughness of FR-SWSSC. The hybrid fibers employed micro and macro fibers, combining them based on size and type, and then compared their impact on the fracture performance of FR-SWSSC with the mixes containing mono fibers. The findings of this study contribute to sustainability in the construction industry by addressing common problems associated with SWSSC.

2. Test program

2.1. Materials

In line with previous findings on the benefits of ground granulated blast furnace slag (GGBS) in lowering CO_2 emissions and enhancing material properties [47–49], this study employed a similar approach. A combination of 35 % ordinary Portland cement (OPC) and 65 % GGBS was used as the cementitious material in all investigated mixes. Ion chromatography (IC) analysis revealed significantly elevated chloride (Cl^-) and sulphate (SO_4^{2-}) concentrations in seawater compared to tap-water [17]. Chloride levels in seawater were approximately 360 times higher than those in tap water, measuring 19,809.7 mg/L and 54.9 mg/L, respectively. Similarly, sulfate concentrations were 76 times greater in seawater (2824.4 mg/L) than in tap-water (36.8 mg/L). The physical properties of coarse aggregate, normal sand, and sea-sand are listed in Table 1. The corresponding sieve analysis for the aggregates is shown in Fig. 1.

Table 2 provides the physical properties of the fibers employed in this study. A combination of synthetic fibers (PP and PVA) and a natural fiber (BF) was used to reinforce SWSSC. The purpose of using these fibers was their readily availability in Australian market and to reduce manufacturing costs while utilizing their high performance. The selection of BF stemmed from its excellent mechanical properties, high-temperature resistance, acid/alkali resistance, readily available raw materials, and eco-friendly processing [50, 51]. Two fiber sizes were investigated including micro-fibers (PPS, PVA, and BF) and macro-fibers (PPL and TPPL), as shown in Table 2. Additionally, recycled plastic-based PPL fibers were incorporated for eco-friendliness. Fiber morphology was characterized using scanning electron microscope (SEM) and presented in Fig. 2.

2.2. Mix design, and specimens preparation

A total of 23 concrete mixes (target compressive strength = 25 MPa) were prepared including two plain concrete (FWNS and SWSS), and 21 FR-SWSSC. The mix proportions and their 28-day compressive strengths (average of three standard cylinders) are presented in Table 3. All concrete mixes shared the same base proportions, with variations only in fiber type and the use of SW and SS. The study incorporated micro-fibers (PPS, PVA, and BF) and macro-fibers (PPL and TPPL) at a total volume of 0.25 %, used in both mono and hybrid configurations (detailed in Table 3). This relatively lower fiber dosage ensured that the performance of samples would not be adversely affected by improper mixing. This percentage aligns with previous studies examining the impact of fibers on various properties of FRC for both FWNSC and SWSSC [17, 21, 30]. Hybrid mixtures incorporated these fibers at ratios of 33 % and 66 % each. For instance, two mixtures were prepared to examine the hybrid behavior of PPL and PVA fibers: 0.33PPL/0.66PVA, and 0.66PPL/0.33PVA. To facilitate the placement of the concrete for the structural applications, a highly workable mix was designed to reach a slump value of 150–200 mm without the use of any superplasticizer.

Table 1
Physical properties of the aggregates.

Material	Specific Gravity (kg/m^3)	Bulk Density (kg/m^3)	Fineness Modulus
Coarse Aggregate	2.71	1560	6.92
Normal Sand	2.66	1628	1.97
Sea-Sand	2.57	1578	1.38

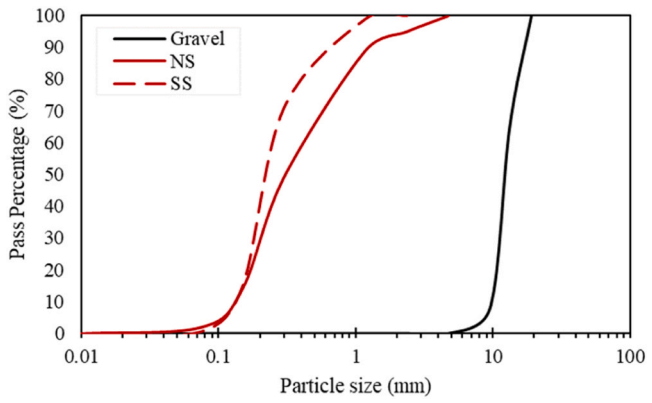

Fig. 1. Grading curves for NS and SS coarse aggregates.

Table 2
Physical properties of different fibers [31].

Property	PPS	PVA	BF	PPL	TPPL
Specific gravity	0.91	1.3	1.57	0.91	0.91
Length (mm)	6	8	7	47	54
Diameter (μm)	180	38	15	—	800
Thickness (μm)	—	—	—	<500	—
Tensile strength (MPa)	600	1600	2900	400	620
Young's modulus (GPa)	9.5	40	85	6	9.5
Chemical resistance	Excellent	Excellent	Excellent	Excellent	Excellent
Melting point (°C)	160	225	1450	160	160
Water absorption (% by weight)	<1	<1	<1	Nil	Nil
Alkali resistance	Excellent	Excellent	—	Excellent	Excellent
Corrosion resistance	Excellent	Excellent	Excellent	Excellent	Excellent

2.3. Test specimens and methods

Three concrete beam specimens were prepared according to Australian Standard AS 1012.2 [52] with dimensions of 100 mm × 100 mm × 350 mm. After casting, beam samples were demolded at 24 h and cured in a moist environment at 23 ± 2°C for one day. Subsequently, they were immersed in a lime-saturated water bath for 28 days, following the same curing procedure as the cylinder samples. After curing, all samples were pre-cracked with a length of 30 mm and a width of 5 mm using a cutting saw, creating a defined notch. To determine the fracture toughness properties, three-point bending test was employed, which have been used widely in previous studies [30, 42, 53–55]. Details regarding the beam geometry and support configuration are provided in Fig. 3. The experiments were conducted with a 100-kN displacement-control testing machine at a loading rate of 0.05 mm/min. A dynamic extensometer and linear variable displacement transducers (LVDT) (see Fig. 3) were used to measure the crack mouth opening displacement (CMOD) and deflection at the mid-span of the beams, respectively. Data were recorded using a data acquisition system, and the test was terminated when CMOD reached 3.5 mm.

3. Results and discussion

Fig. 4 shows typical failures of the specimens. As expected, all specimens exhibited a major crack forming at the mid-span notch point. With increasing concentrated load, the crack at the concrete mid-span propagated upward, and all specimens exhibited similar Mode I fracture (fracture opening in tension), as anticipated. A detailed analysis of the fracture properties, including load–CMOD curves, fracture energy, and fracture toughness, along with the overall behavior of the specimens, is presented and compared in subsequent sections.

3.1. Load–CMOD curves

Fig. 5a-c presents load-CMOD curves for concrete mixes reinforced with mono-, hybrid micro-, and hybrid macro/micro-fibers, respectively. As shown in Fig. 5a, plain concretes (SWSS and FWNS) showed similar pre-peak behavior with comparable strengths but exhibited brittle failure after cracking (sudden strength loss). All FR-SWSSC mixes exhibited approximately similar initial pre-peak behavior, suggesting minimal fiber contribution in the pre-cracking stage, aligning with prior research findings [30, 42]. Fig. 6 presents the load reduction factor (LRF), defined as the ratio of the peak load to the residual load at 0.8 mm of CMOD. The LRF represents the percentage reduction in load capacity between the peak point and the point where the CMOD reaches 0.8 mm. Both SWSS and FWNS concretes exhibited significant strength loss, exceeding 80 % at 0.8 mm CMOD, with negligible residual strength (defined as post-peak flexural strength) remaining at 2.5 mm CMOD. Macro fiber addition (PPL and TPPL) significantly improved post-cracking behavior in SWSSC, maintaining approximately 50 % and 38 % of peak load at 0.8 mm CMOD, respectively. Among the micro-fibers investigated (PVA, PPS, and BF), PVA exhibited the best post-crack performance (Figs. 5a and 6), potentially due to strong chemical bonding with the matrix, as reported in previous studies [31, 33, 56].

In comparison, as shown in Fig. 5b, the post-cracking behavior of hybrid micro-fiber mixes showed improvement specially when PVA fibers were incorporated in the hybrid system. According to Fig. 5b, the hybrid PVA/PPS fibers significantly improved LRF compared to both mono PVA and PPS fibers. In this case, incorporating 0.66PPS/0.33PVA was more effective. Additionally, compared to mono BF, PVA/BF and PPS/BF hybridization significantly improved LRF and maintained the load drop after peak point. At a CMOD of 0.8 mm, hybrid 0.66PVA/0.33BF fibers showed a great enhancement of strength, with an approximately 185 % and 55 % increase compared to mono BF and plain SWSSC, respectively. This improvement can be attributed to the chemical bonding between PVA and BF fibers [31, 34, 56], which enhanced the strength of the mixture by increasing its cohesion and overall strength, resulting in improved peak-load and post-cracking performance.

Micro/macro fiber hybridization (Fig. 5a) improved both peak and post-cracking performance in all fiber mixtures. This is attributed to macro-fibers bridging cracks, enhancing the load-carrying capacity of SWSSC. Their longer length allows macro-fibers to limit crack width more effectively than micro-fibers. Among the hybrids, 0.66PPL/0.33PVA improved flexural strength by 10 % compared to mono PVA, while 0.33PPL/0.66BF yielded a 20 % increase compared to mono BF. Fig. 6 demonstrates significant improvement in LRF and post-peak behavior of SWSSC due to hybrid macro/micro fiber incorporation. PPL/PPS hybridization yielded the greatest improvement in LRF, with a 193 %–273 % enhancement compared to mono PPS fibers. This superior performance stems from the effectiveness of long PPL fibers in bridging post-peak macro cracks. Compared to mono PVA and BF, both hybrid PPL/PVA and PPL/BF significantly enhanced the ratio by 47–77 %, while TPPL/PVA and TPPL/BF achieved a 55–115 % improvement. This enhancement was likely attributed to the improved bonding strength of PPL and TPPL fibers achieved through hybridization with PVA and BF fibers. Considering the SEM images in Fig. 7, the hybrid PPL/PVA and TPPL/PVA fibers appear to exhibit synergistic effects. This stems from the strong chemical bonds between PVA and BF and the SWSSC matrix, as reported previously [30, 31]. Notably, TPPL/PVA exhibited the highest improvement, likely due to superior TPPL fiber distribution and flexibility compared to PPL.

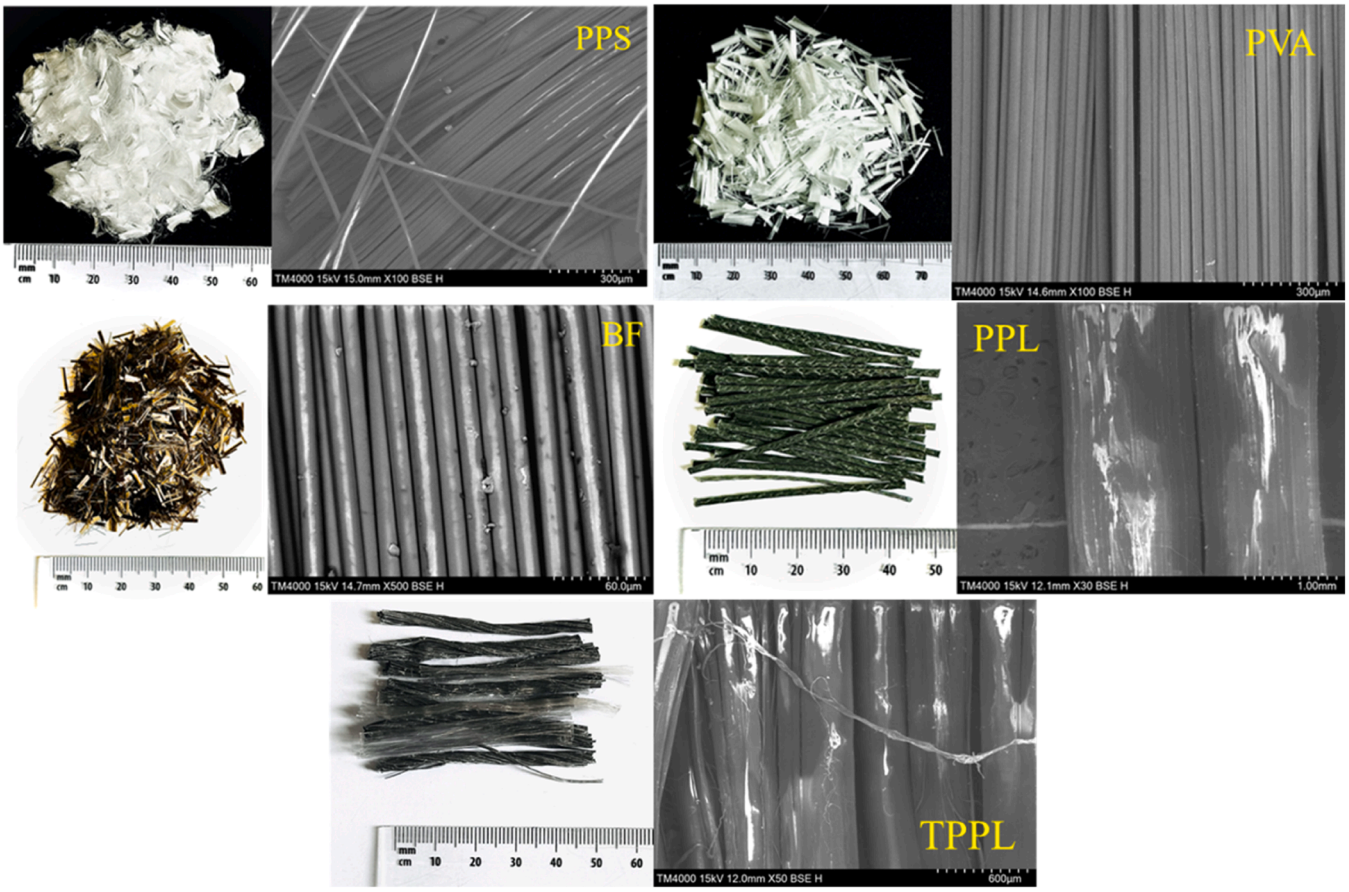

Fig. 2. Characterization of various fibers: shape, dimensions, and SEM images.

Table 3
Concrete mix design and their 28-day compressive strengths.

Groups	Concrete Mix	Binder (kg/m^3)		Gravel (kg/m^3)	Sand (kg/m^3)		Water (kg/m^3)		Fiber (kg/m^3)					28-day f'_C (MPa)
		OPC	GGBS		NS	SS	FW	SW	PPS	PVA	BF	PPL	TPPL	
Plain	FWNS	126	234	995	785	—	256	—	—	—	—	—	—	28.5
	SWSS	126	234	995	—	785	—	256	—	—	—	—	—	27.6
Mono	PPS	126	234	995	—	785	—	256	2.28	—	—	—	—	27.2
	PVA	126	234	995	—	785	—	256	—	3.25	—	—	—	28.9
	BF	126	234	995	—	785	—	256	—	—	6.63	—	—	27.4
	PPL	126	234	995	—	785	—	256	—	—	—	2.28	—	28.6
	TPPL	126	234	995	—	785	—	256	—	—	—	—	2.28	29.0
Hybrid micro	0.33PPS/0.66BF	126	234	995	—	785	—	256	0.76	—	4.41	—	—	27.9
	0.66PPS/0.33BF	126	234	995	—	785	—	256	1.52	—	2.21	—	—	28.2
	0.66PVA/0.33BF	126	234	995	—	785	—	256	—	2.17	2.21	—	—	31.1
	0.33PVA/0.66BF	126	234	995	—	785	—	256	—	1.08	4.41	—	—	27.0
	0.33PPS/0.66PVA	126	234	995	—	785	—	256	0.76	2.17	—	—	—	27.3
	0.66PPS/0.33PVA	126	234	995	—	785	—	256	1.52	1.08	—	—	—	26.9
Hybrid macro/micro	0.33PPL/0.66PPS	126	234	995	—	785	—	256	1.52	—	—	0.76	—	27.2
	0.66PPL/0.33PPS	126	234	995	—	785	—	256	0.76	—	—	1.52	—	26.4
	0.66PPL/0.33PVA	126	234	995	—	785	—	256	—	1.08	—	1.52	—	31.9
	0.33PPL/0.66PVA	126	234	995	—	785	—	256	—	2.17	—	0.76	—	31.1
	0.33PPL/0.66BF	126	234	995	—	785	—	256	—	—	4.41	0.76	—	31.5
	0.66PPL/0.33BF	126	234	995	—	785	—	256	—	—	2.21	1.52	—	31.5
	0.33TPPL/0.66PVA	126	234	995	—	785	—	256	—	2.17	—	—	0.76	30.3
	0.66TPPL/0.33PVA	126	234	995	—	785	—	256	—	1.08	—	—	1.52	30.5
	0.33TPPL/0.66BF	126	234	995	—	785	—	256	—	—	4.41	—	0.76	28.5
	0.66TPPL/0.33BF	126	234	995	—	785	—	256	—	—	2.21	—	1.52	29.6

3.2. Fracture energy (G_F)

In this study Eq. 1, [57] was adopted to calculate fracture energy (G_F). Researchers commonly employ this equation to quantify total energy dissipation per unit crack area from load-CMOD curves [58–60].

$$G_F = \frac{0.75W_0 + W_1}{A_{lig}} \quad (1)$$

In Eq. 1, W_0 denotes the energy consumed at CMOD=3.5 mm and A_{lig} represents the ligament area. The work W_1, due to self-weight of the

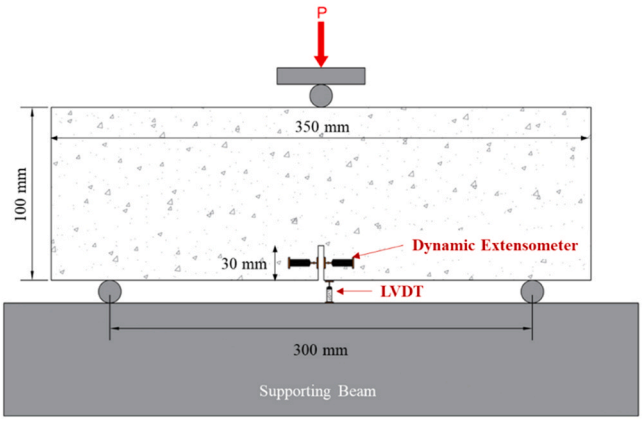

Fig. 3. Schematic of the fracture toughness test setup.

Fig. 4. Typical fracture toughness failure mode.

specimen and equipment (e.g., steel rod), is calculated as:

$$W_1 = 0.75 \times \frac{S}{L} m \times g \times CMOD_c \quad (2)$$

with S as the loading span, L the specimen length, m the specimen mass, and g representing the gravity acceleration, and $CMOD_c$ = 3.5 mm.

Fig. 8 presents the mean G_F values for all investigated concrete mixes at CMOD values of 0.5, 1.0, and 3.5 mm. The results demonstrated approximately similar G_F values for both FWNS and SWSSC across all CMOD values. The incorporation of mono fibers exhibited a dependence on fiber type, with increases or decreases in G_F observed. Notably, mono fibers were more effective at higher CMOD values due to their ability to bridge the load across cracked concrete. For example, PPS and BF fiber incorporation significantly decreased G_F, while PPL and TPPL fibers significantly improved it. PPL and TPPL fibers demonstrably increased G_F by approximately 144 % and 93 %, respectively, compared with plain SWSSC at a CMOD of 3.5 mm. Mono PVA fiber incorporation resulted in lower G_F at lower CMOD values, but it increased at a CMOD of 3.5 mm by about 11 %. The observed behavior could be due to the crack-bridging capability of PVA fibers, which stems from their superior bonding and tensile strengths. However, their effectiveness in this

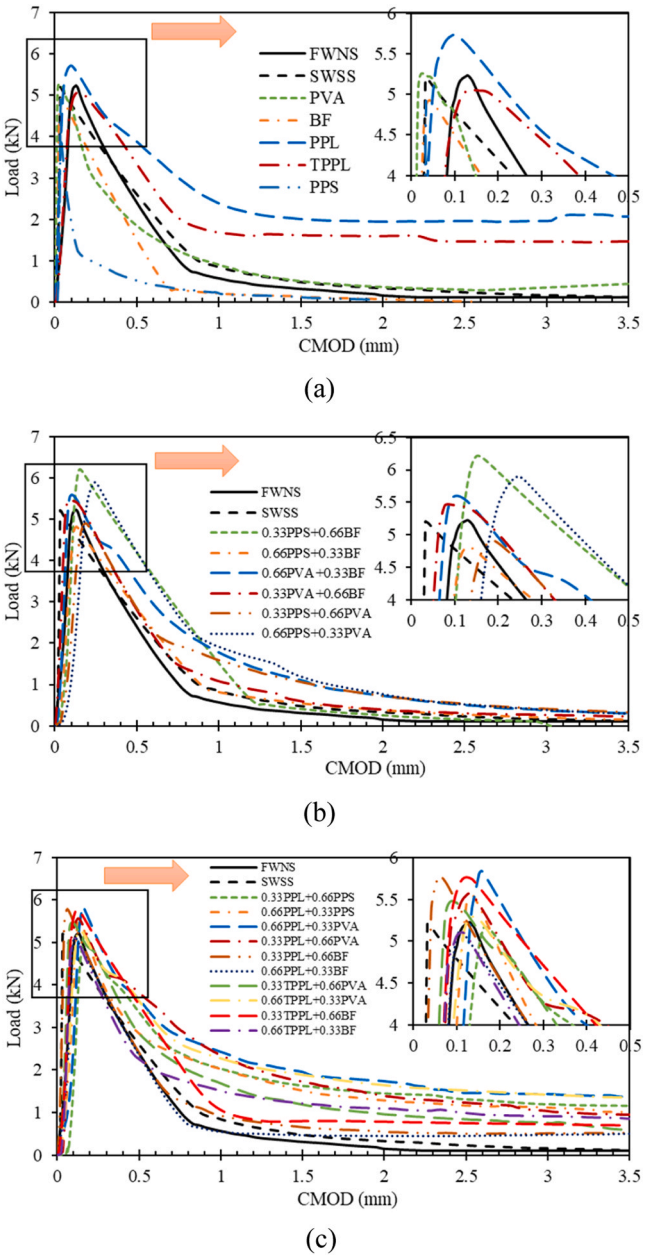

Fig. 5. Load-CMOD curves of flexural strength test for different fiber types: (a) Mono-fibers, (b) Hybrid micro-fibers, (c) Hybrid micro- and macro-fibers.

regard is demonstrably lower compared to PPL and TPPL fibers, likely due to a difference in fiber length.

The combination of micro-fibers significantly influenced G_F and exhibited a synergistic effect compared to mono fibers. Hybridizing PPS with BF or PVA significantly improved G_F at CMOD 3.5 mm by approximately 176 % and 290 %, respectively, compared to mono PPS. Additionally, hybrid PPS/PVA fiber was more effective than hybrid PPS/BF fiber, which led to an increased G_F at CMOD 3.5 mm by 53 % over mono PVA. Notably, a higher dosage of BF in the hybrid system with PPS fibers (0.33PPS/0.66BF) proved more effective, while for PVA and PPS hybridization, a higher dosage of PPS fibers (0.66PPS/0.33PVA) yielded better results. These observations can be attributed to the ability of PVA and BF fibers to enhance the bonding strength of PPS fibers. While BF exhibited slight corrosion in SWSSC [31], leading to their lower contribution to improved bonding compared to PVA fibers, a higher dosage of BF was required in the hybrid system. When it comes to the PVA/BF hybrid, G_F at CMOD 3.5 mm improved by 62 % compared to

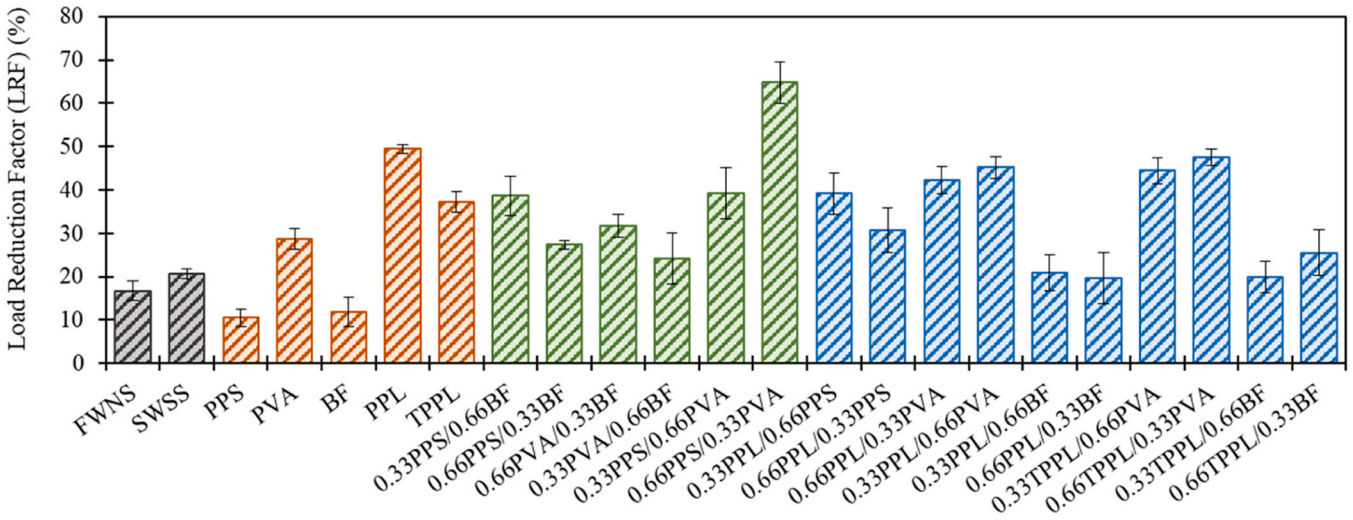

Fig. 6. Comparison of load reduction factor (LRF) values for different concrete mixes.

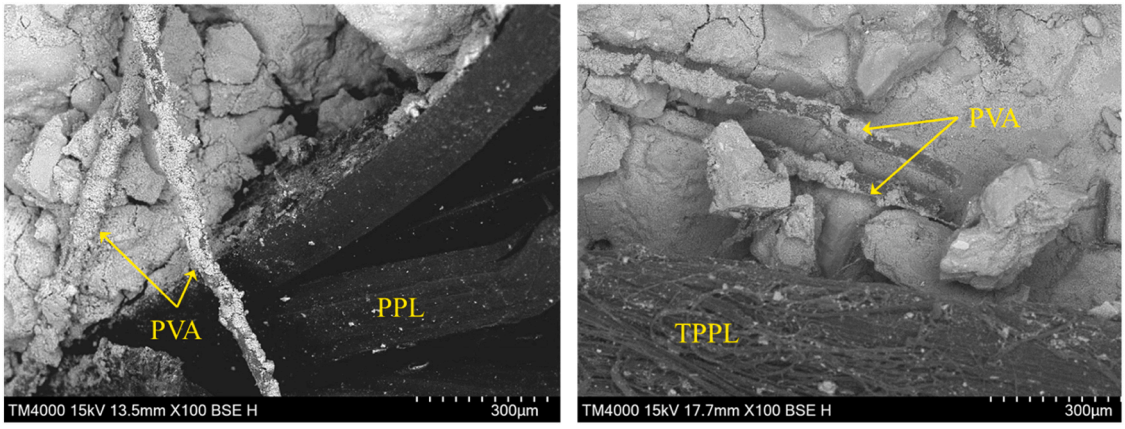

Fig. 7. The SEM images of hybrid PPL/PVA and TPPL/PVA fibers.

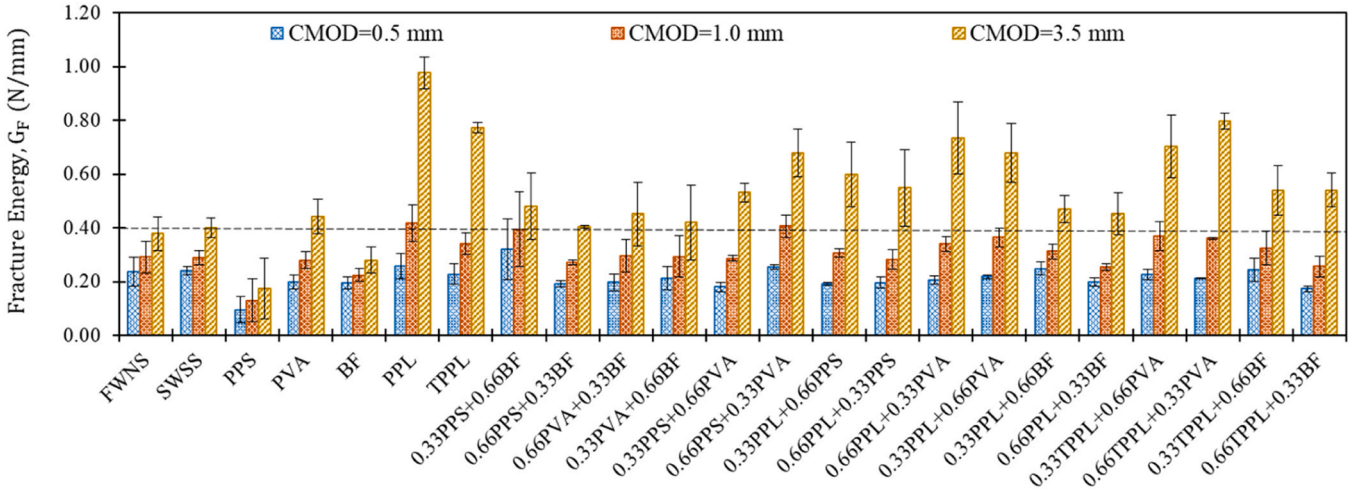

Fig. 8. Comparison of fracture energy for different concrete mixes.

mono BF incorporation. In this case, 0.66PVA/0.33BF was more effective.

A significant improvement in G_F was observed for all CMOD values when macro/micro fiber hybridization was employed compared to mono PPS and BF. This enhancement was attributed to the bridging effect of macro fibers across larger cracks, with its effectiveness increasing with higher CMOD values. Specifically, hybridization of PPL fibers with PPS, PVA, or BF resulted in increases of 244 %, 66 %, and

68 % in G_F at a CMOD of 3.5 mm, respectively, compared to only micro-fibers. Similarly, hybridization of TPPL with PVA or BF led to enhancements of 80 % and 93 % in G_F at a CMOD of 3.5 mm, respectively. Notably, a fiber volume fraction of 0.66TPPL/0.33PVA (or BF) and 0.66PPL/0.33PVA (or BF) proved to be more effective.

In summary, the fracture energy analysis revealed a positive correlation with increasing CMOD value. This trend was attributed to the enhanced contribution of macro-fibers (due to their extended length and mechanical bonding) and micro-fibers (particularly PVA and BF with superior chemical bonding and tensile strength) in arresting crack propagation. Notably, fiber length emerged as the most crucial parameter influencing G_F improvement.

3.3. Fracture toughness (K_{IC})

In three-point bending fracture tests, concrete undergoes three stages including crack initiation, stable crack propagation, and critical unstable fracture. The double-K fracture model (DKFM), a two-parameter method for assessing concrete fracture behavior [61–64], treats it as a brittle elastic-plastic material. It defines K_{IC}^{ini} (initial fracture toughness) as the energy for crack initiation influenced by cohesive strength, and K_{IC}^{un} (unstable fracture toughness) as the energy for continued crack propagation governed by tensile strength. DKFM allows evaluation of concrete fracture behavior under varying loads and the influence of reinforcement. This study employs DKFM to calculate fracture parameters of the investigated mixtures, with results presented in this section.

According to the DKFM (Fig. 9), the K_{IC}^{ini} can be calculated using Eq. (3).

$$K_{IC}^{ini} = \frac{3(P_{ini} + \frac{mg}{2})S\sqrt{a_0}}{W^2 B} f(V_0) \tag{3}$$

where S denotes the span length. For S/W values of 2.5 and 4.0, the function $f(V_0)$ can be determined using Eqs. (4) and (5), respectively. Interpolation techniques can then be employed to estimate $f(V_0)$ for intermediate S/W ratios.

$$f(V_0) = \frac{1.83 - 1.65V_0 + 4.76{V_0}^2 - 5.3{V_0}^3 + 2.51{V_0}^4}{(1+2V_0)(1-V_0)^{3/2}} \tag{4}$$

$$f(V_0) = \frac{1.99 - V_0(1-V_0)(2.15 - 3.93V_0 + 2.7{V_0}^2)}{(1+2V_0)(1-V_0)^{3/2}} \tag{5}$$

where P_{ini} represents the initial cracking load; W denotes the height of the beams; B represents the width of the beams; a_0 represents the length of the initial crack; and V_0 represents the ratio of the initial crack length to the depth of the specimen (a_0/W).

Using Eq. (6), K_{IC}^{un} can be calculated.

$$K_{IC}^{un} = \frac{3(P_{\max} + \frac{mg}{2})S\sqrt{a_C}}{W^2 B} f(V_C) \tag{6}$$

where a_C represents the critical effective crack length, and it can be calculated using Eq. (7) as follows:

$$a_C = \frac{2}{\pi}(W + H_0)arctg\sqrt{\frac{B.E.CMOD_C}{32.6P_{\max}} - 0.1135} - H_0 \tag{7}$$

where $P_{\max}$ represents the peak load, $CMOD_C$ represents the critical crack mouth opening displacement, H_0 refers to the thickness of the knife edges, and E denotes the elastic modulus, which can be calculated using Eq. (8).

$$E = \frac{1}{BC_i}\left[3.7 + 32.6\tan^2\left(\frac{\pi}{2}\frac{a_0 + H_0}{W + H_0}\right)\right] \tag{8}$$

where, C_i, representing the initial compliance, can be expressed as $CMOD_i/P_i$, and P_i is the load at the initial linear segment of the P-CMOD curve. When $S/W = 2.5$ and 4.0, $f(V_C)$ can be calculated using Eqs. (9) and (10), respectively [61, 62, 65, 66].

$$f(V_C) = \frac{1.83 - 1.65V_C + 4.76{V_C}^2 - 5.3{V_C}^3 + 2.51{V_C}^4}{(1+2V_C)(1-V_C)^{3/2}} \tag{9}$$

$$f(V_C) = \frac{1.99 - V_C(1-V_C)(2.15 - 3.93V_C + 2.7{V_C}^2)}{(1+2V_C)(1-V_C)^{3/2}} \tag{10}$$

The span-to-height ratio of the beams, denoted as V_C, can be calculated by taking the ratio of a_C/W. In this study, the span-to-height ratio (S/W) of the specimen used in the fracture test was designed to be 3.0. As a result, $f(V_0)$ and $f(V_C)$ must be obtained through linear interpolation using the values calculated using S/W values of 2.5 and 4.

The cohesion toughness, represented by K_{IC}^{C}, can be considered as the energy absorbed in the progressive expansion of the fracture process zone. As such, it can be evaluated by utilizing the following straightforward relationship:

$$K_{IC}^{ini} = K_{IC}^{un} - K_{IC}^{C} \tag{11}$$

where K_{IC}^{C} represents the cohesion toughness that arises from the cohesive force within the fracture process zone (FPZ), a region around the crack tip where there is localized damage.

Fig. 10 depicts higher initial fracture toughness (K_{IC}^{ini}) for SWSSC compared to FWNS concrete (by approximately 7 %), likely due to its denser pore structure as supported by [21, 31, 67], which may reduce initial microcracking. The SEM analysis in Fig. 11 provides further evidence for the denser structure of SWSSC compared to FWNS. As K_{IC}^{ini} reflects inherent toughness at crack initiation, this denser structure likely reduces microcracking at the initial stages, potentially explaining the increased K_{IC}^{ini}. However, K_{IC}^{un} results indicate a 12 % lower value for SWSSC. Similarly, Fig. 12 shows a significant reduction (by approximately 96 %) in K_{IC}^{C} for SWSS compared to FWNS. These findings suggest that while the denser structure in SWSS enhanced initial crack resistance, it may also promote a more brittle fracture behavior within the FPZ, leading to lower K_{IC}^{C}.

Mono-fiber mixtures exhibited lower K_{IC}^{ini} compared to plain SWSSC, with PPS fibers showing the least reduction. This is likely due to microcrack formation within the matrix, which weakens the dense structure of plain SWSSC. However, these microcracks can dissipate stress and prevent larger cracks, leading to significantly higher K_{IC}^{un}—a measure of total toughness near failure—with mono PVA and PPL fibers increasing it by 24 % and 51 %, respectively, compared to plain SWSSC. PPS fiber incorporation demonstrated the least reduction in initial fracture toughness (K_{IC}^{ini}) but proved ineffective for ultimate fracture toughness (K_{IC}^{un}). This behavior likely arises from the inherent properties of PPS fibers. Their lower stiffness and tensile strength compared to other fibers might improve initial crack resistance through microcrack bridging, but hinder crack arrest and strength enhancement due to weak concrete-fiber bonding, promoting fiber pull-out instead of breakage. Conversely, strong chemical bonding in PVA fibers and superior me-

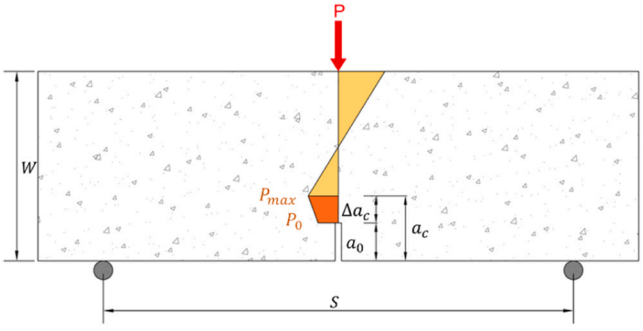

Fig. 9. Stress distribution of DKFM method.

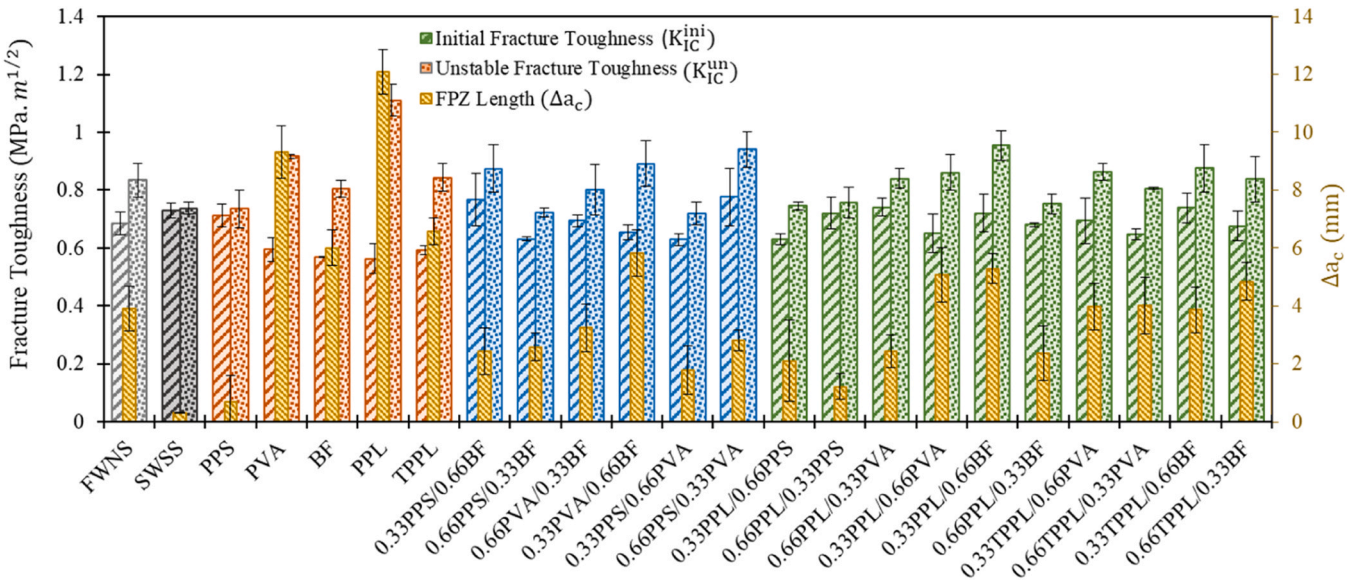

Fig. 10. The fracture toughness properties (initial and unstable) based on DKFM method.

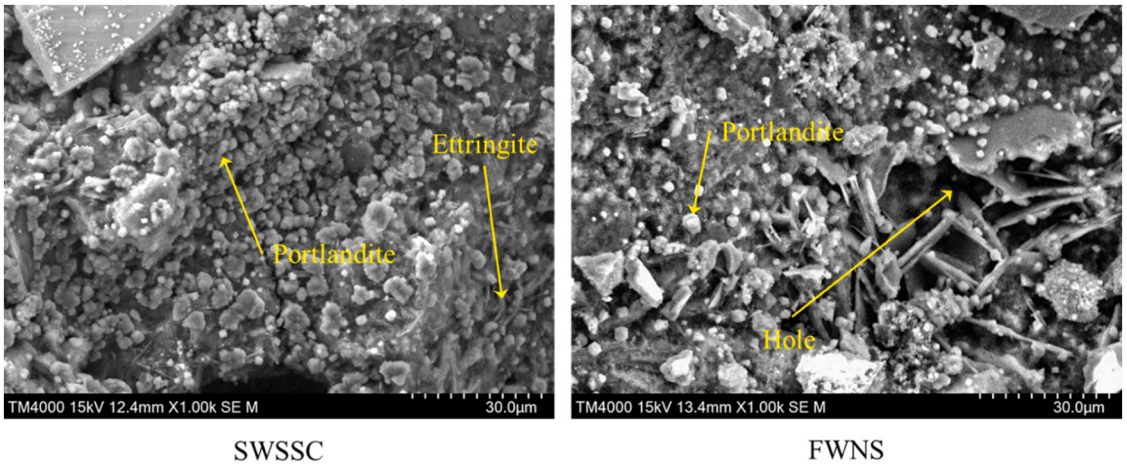

Fig. 11. The microstructure of plain concrete mixtures (FWNS and SWSS) using SEM images.

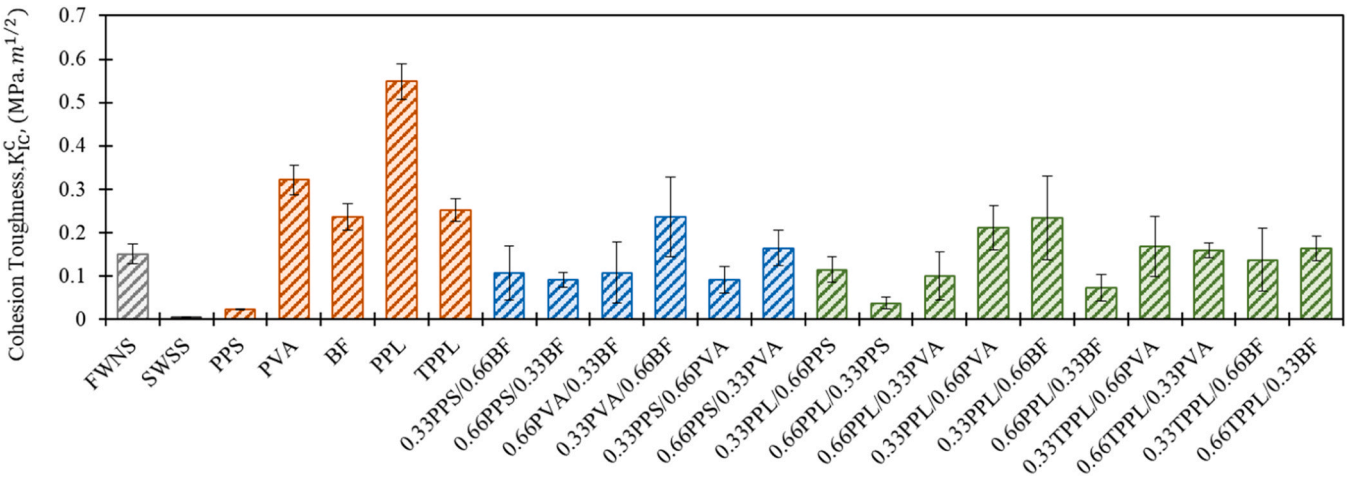

Fig. 12. The cohesion toughness (K_{IC}^{C}) parameter based on DKFM method.

chanical interlocking in PPL and TPPL fibers with the concrete matrix resulted in higher K_{IC}^{un}. This is further supported by the K_{IC}^{C} results in Fig. 12, where PPS fiber exhibited the lowest value. Overall, fiber addition significantly improved the K_{IC}^{C} of SWSSC, with PVA and PPL fibers being most effective, leading to approximately 54 and 93 times higher K_{IC}^{C}, respectively.

Micro-fiber hybridization significantly increased K_{IC}^{ini} compared to mono-fiber mixtures. Notably, 0.66PVA/0.33BF hybridization yielded the greatest improvement, surpassing both BF and PVA by 22 % and 17 %, respectively. This is attributed to the positive synergy of PVA/BF in SWSSC, enhancing chemical bonding with the matrix and promoting more efficient reinforcing. Hybridizing PPS with BF or PVA significantly improved fracture behavior compared to mono PPS. Hybrid 0.33PPS/0.66BF and 0.66PPS/0.33PVA increased K_{IC}^{ini} (by about 8 % and 9 %), K_{IC}^{un} (by about 19 % and 28 %), and K_{IC}^{C} (by about 362 % and 616 %), respectively, over mono PPS. This improvement likely stemmed from enhanced bonding strength of PPS fibers, a key weakness, due to the incorporation of PVA or BF, which exhibit strong adhesion to the concrete matrix. Incorporation of hybrid 0.33PPS/0.66BF and 0.66PPS/0.33PVA fibers led to increases in K_{IC}^{ini} (by about 35 % and 31 %) and K_{IC}^{un} (by about 9 % and 3 %) compared to mono BF and PVA fibers. Conversely, a significant decrease in K_{IC}^{C} (by about 55 % and 49 %) was observed compared to mono BF and PVA fibers. This suggests that BF and PVA fibers enhance the bonding of PPS fibers within the concrete matrix, resulting in improved energy absorption, crack bridging capacity, and overall fracture behavior.

Macro/micro-fiber hybridization significantly increased K_{IC}^{ini} compared to mono-fiber. PPL or TPPL combined with BF or PVA fibers showed the most pronounced effect. For example, 0.66PPL/0.33PVA hybridization increased K_{IC}^{ini} by 25 % and 32 % over mono-PVA and PPL, respectively. Similarly, 0.33PPL/0.66BF increased K_{IC}^{ini} by 27 % and 28 % over mono-BF and PPL, respectively. The results showed that 0.33PVA was more effective in the PPL fiber-containing hybrid system, while 0.66BF proved more effective in the combined PPL/BF system. Notably, both micro-fiber type and dosage significantly influenced the initial crack strength. The difference in effectiveness between PVA and BF in SWSS is attributed to their bonding behavior. PVA fibers exhibited strong chemical bonding [17, 31], enhancing the adhesion of PPL fibers by reinforcing the surrounding matrix. Consequently, a lower dosage (0.33 %) of PVA fibers is sufficient to improve PPL fiber bonding and achieve superior fracture toughness compared to a higher PVA dosage in the hybrid system. Conversely, previous research suggested that BF corrosion in SWSSC can compromise its bridging capability [31, 68, 69]. This necessitates a higher BF content for effective PPL fiber bonding and positive synergy within the hybrid system. Considering the results of K_{IC}^{un}, it was found that macro-fiber type significantly impacted K_{IC}^{un}. A 0.33TPPL/0.66BF configuration yielded 9 % and 4 % greater K_{IC}^{un} compared to mono-fiber and TPPL configurations, respectively. The improved performance may be attributed to a superior distribution of TPPL fibers, enhancing their bond strength with the concrete matrix, particularly when combined with PVA or BF. The results of K_{IC}^{C} indicated that macro/micro-fiber hybridization significantly reduced K_{IC}^{C} compared to mono fibers. The positive synergy between micro and macro fibers enhanced crack resistance across a broad spectrum and improved energy absorption during crack propagation.

FWNS concrete exhibited a 12.6-fold increase in fracture process zone length (Δa_C) compared to SWSSC. This suggests a more brittle behavior and lower damage tolerance for SWSSC. Materials with shorter Δa_C lack the capacity to absorb stress in the surrounding crack zone, potentially leading to rapid crack growth and brittle failure. This may be attributed to the denser microstructure of SWSSC [31], which enhances crack initiation resistance but accelerates subsequent propagation. Mono-fiber addition significantly enhanced Δa_C compared to plain SWSSC. PVA, BF, PPL, and TPPL fibers were particularly effective, increasing Δa_C by 30, 19, 39, and 21 times, respectively. This suggests fibers improved the fracture toughness of SWSSC, transitioning its behavior from brittle to ductile, leading to enhanced damage tolerance and plastic deformation, due to fiber bridging, as corroborated by prior research [30, 61, 70, 71]. Fiber hybridization further increased Δa_C for PPS fibers, addressing their inherent weakness in bonding with the concrete matrix.

3.4. Analysis of fracture behavior

To investigate the fracture behavior of plain concrete and fiber-reinforced SWSSC mixes, load-CMOD curves for previously identified promising mixes are analyzed and presented in Fig. 13. These mixes were selected based on prior fracture analysis results. To further visualize the fracture behavior, schematic failure mode is illustrated in Fig. 14. For improved clarity, the fracture behavior in Fig. 13 is categorized into six stages, which are comprehensively discussed in the following section.

1) O-A: Linear-elastic phase
2) A-B: Crack initiation stage and Crack propagation stage
3) B: Peak load stage
4) B-C: Post-peak stage
5) C-D: Continuation of the post-peak stage
6) D-E: Concrete failure stage

Between points O and A (60–80 % ultimate strength), plain and FR-SWSSC demonstrated linear-elastic behavior with minimal cracks. While both exhibited this behavior, the underlying mechanisms differed. The slope for plain SWSSC reflected its slightly higher elastic modulus than normal concrete by about 8 % due to sea-sand [31]. Conversely, FR-SWSSC exhibited a load-CMOD slope dependent on fiber characteristics (type, volume fraction, aspect ratio, distribution, and hybridization). Though fibers potentially increased tensile strength in both plain and FR-SWSSC, they primarily influenced crack behavior in FR-SWSSC by delaying initiation and reducing initial width. During this initial stage, no fibers were activated, and overall behavior (except stiffness) remained similar.

The concrete specimens exhibited a transition from the linear elastic to crack initiation and propagation stages (A-B). Both SWSS and FR-SWSSC displayed non-linear behavior with increasing crack width (CMOD). SWSSC deviated from linearity during crack initiation due to its lower tensile strength, resulting in rapid crack growth during propagation as the material could not sustain the load. The load-CMOD curve of FR-SWSSC exhibited a deviation from linearity during crack initiation. This behavior can be attributed to the influence of fiber type, volume fraction, aspect ratio, distribution, and hybridization. These fibers bridged crack tips, delaying initiation, and resulting in a slight load increase and reduced initial crack width. Fibers inhibited crack growth during propagation, significantly reducing crack width and increasing

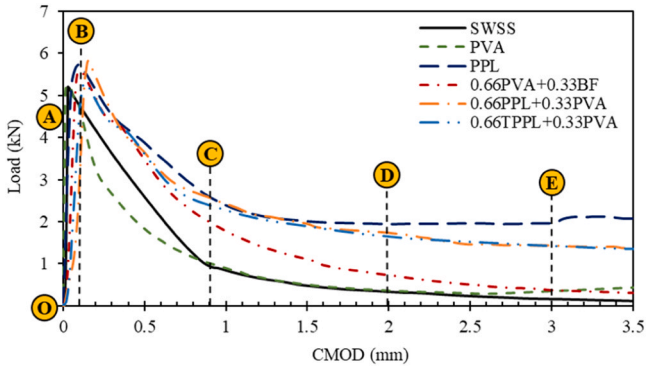

Fig. 13. Load-CMOD curves for various SWSSC mixes.

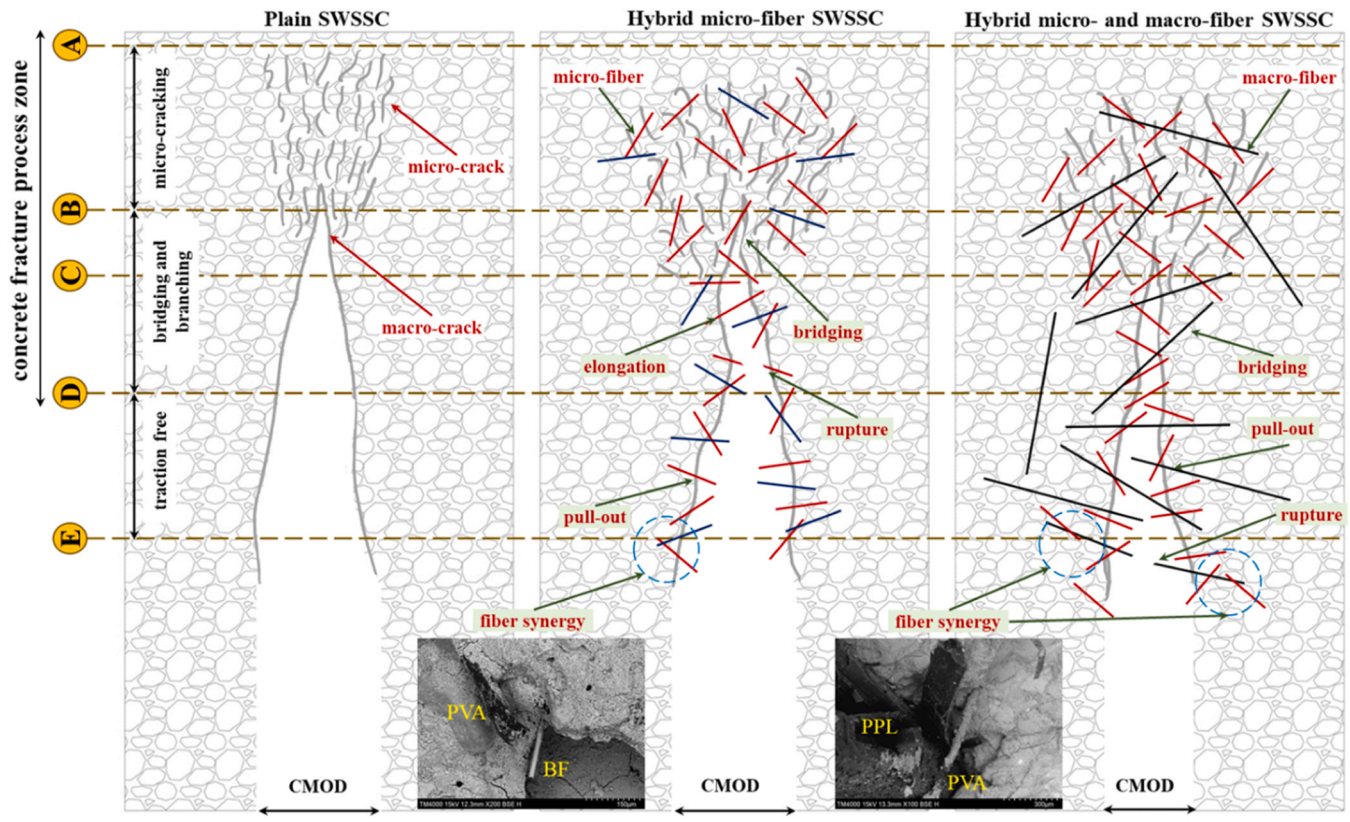

Fig. 14. Schematic of the crack development process in hybrid FR-SWSSC.

peak load. PVA fibers exhibited stronger bonding with concrete matrix, while PPL fibers, with their superior length, enhanced bridging, and fracture energy. Notably, all hybrid mixtures displayed a higher ultimate load compared to those containing only PVA fibers. Additionally, replacing 33 % of PVA with BF fibers significantly improved fracture behavior during this stage. This improvement could stem from the positive synergy of PVA/BF hybridization, where BF enhanced the bonding strength of PVA fibers by reinforcing the surrounding concrete matrix, thereby facilitating greater contribution from the PVA fibers. This complementary mechanism can be observed in Fig. 14 through SEM imaging.

Following the peak load stage, concrete specimens transitioned to the post-peak stage (B-C), marked by a sudden localization and propagation of a macrocrack through the beam, leading to a significant loss in flexural strength. Plain SWSSC displayed a post-peak decrease in load capacity and load-CMOD curve, driven by its low tensile strength. Aggregate bridging acted as the main toughening mechanism. With diminishing load resistance, the crack width continued to increase. The post-peak stage in FR-SWSSC also exhibited a decrease in load capacity, although the rate of decrease was influenced by fiber type. Fibers enhanced the tensile strength of SWSSC, leading to a higher residual strength at Point C and a reduced rate of crack width increase compared to plain concrete. Fiber hybridization significantly improved load-bearing capacity compared to mono PVA fibers. Notably, the 0.66PVA/0.33BF combination enhanced both bonding strength and the bridging effect within the hybrid system, leading to a higher load capacity. Similarly, a 0.33PVA content in hybrids with 0.66PPL or 0.66TPPL improved the bonding of macro-fibers (PPL and TPPL), consequently resulting in a significantly enhanced bridging effect. The strong chemical bonding strength of PVA fibers significantly reinforced the surrounding concrete of macro-fibers (Fig. 14). Furthermore, the higher mechanical bonding strength of PPL fibers compared to TPPL fibers, attributed to their rough surface, resulted in a better synergistic effect with PVA fibers, enhancing the ultimate capacity relative to TPPL/PVA hybridization. Moreover, the residual strength of Point C highlighted the crucial role of macro-fibers in maintaining post-peak load.

Specimens with macro-fibers exhibited a slower load-CMOD reduction and reached stability during transition from point C to D. This extended softening, attributed to crack-bridging and branching, contrasted with the failure-prone behavior of plain SWSSC due to its loosely connected aggregates, leading to rupture or pull-out of fibers. Conversely, the 0.66 PVA/0.33BF mix, displayed rapid crack widening and reduced load capacity, attributed to lacking elongation-providing fibers like PPL or TPPL. However, its higher capacity compared to plain SWSSC can be explained by a strong bond between PVA, BF, and the concrete matrix. At large CMOD values during this phase, macro-fibers exhibited a more pronounced influence on crack propagation arrest and stabilization due to their greater length. However, their synergistic interaction with microfibers, particularly PVA and basalt BF, yielded superior performance compared to micro-fibers alone. The incorporation of mono micro-fibers proved inadequate in sustaining crack growth at large CMOD values, owing to their limited length and tensile strength.

During the failure stage (D to E and after), SWSSC and FR-SWSSC exhibited distinct failure mechanisms under load. SWSSC experienced a sudden, brittle failure with complete load-bearing capacity loss and minimal energy dissipation. The failure mode was typically tensile, with concrete fracturing along cracks. On the other hand, FR-SWSSC failure can be impacted by fiber properties, potentially experiencing delays due to increased energy absorption within the fibers. These fibers also altered the failure mode from brittle to ductile, allowing concrete deformation before catastrophic failure. Among the fiber types, macro-fibers offered consistent load-bearing capacity, while single PPL fibers exhibited enhanced energy absorption and a slight improvement in load-bearing. The PVA/BF hybrid, however, reached its minimum load capacity due to short length and inability to bridge macrocracks. These findings highlight the crucial role of macro-fibers in enhancing the ductility of FR-SWSSC.

3.5. Post-crack performance evaluation using guidelines

The post-crack behavior of FR-SWSSC was investigated in this study to elucidate its residual strength and brittleness, providing more insights to informing the design and evaluation of FR-SWSSC structures. Established methods outlined in the Fib Model Code [72], European standard EN 14651 [73], and RILEM TC 162-TDF [74] are employed. The study focused on determining residual strength corresponding to specific CMOD of 0.5, 1.5, 2.5, and 3.5 mm, following the Fib Model Code [69] (Fig. 15). Residual strength was evaluated using f_{R1} and f_{R3} for both serviceability (SLS) and ultimate (ULS) limit states. Moreover, the f_{R3}/f_{R1} ratio assessed material brittleness. The potential for FR-SWSSC to partially replace ULS reinforcement if it meets $f_{R1}/f_L > 0.4$ and $f_{R3}/f_{R1} > 0.5$ [72, 75]. f_L, defined by RILEM TC 162-TDF [74] and EN 14651 (CEN 2005) [73], is the peak load within 0–0.05 mm of CMOD. The flexural strengths were calculated using:

$$f_r = \frac{3}{2}\frac{F \times S}{b \times h_{sp}^2} \tag{12}$$

where F represents load values from tests, b is the specimen width (100 mm), and h_{sp} is the distance from notch tip to the top of the cross-section (70 mm).

Fig. 16 presents the flexural strength of all investigated mixtures. FWNS and SWSS measured 4.94 MPa and 4.79 MPa, respectively. Mono fiber addition to SWSS minimally affected peak strength, except for PPL fibers, which increased it by 10 %. Micro-fiber hybridization with 0.66PPS/0.33PVA achieved the highest strength (5.74 MPa), exceeding mono PPS and PVA by 26 % and 22 %, respectively. This was likely due to the superior chemical bonding of PVA fibers, enhancing the bonding strength of PPS fibers within the concrete matrix. Incorporation of hybrid micro- and macro-fibers including 0.66PPL/0.33PVA, 0.33PPL/0.66BF, and 0.33TPPL/0.66BF, significantly enhanced SWSS flexural strength by about 8 %, 14 %, and 8 %, respectively, compared to plain SWSS. These mixtures also exhibited greater strength than mono PVA and BF.

Fig. 17 shows the residual strength ratios (f_{R3}/f_{R1} and f_{R1}/f_L), with f_{R3}/f_{R1} indicating material brittleness. Mono PPL and TPPL fibers increased f_{R3}/f_{R1} by 317 % and 278 %, respectively, compared to plain SWSSC, resulting in significantly more ductile behavior. Among the micro-fibers, only PVA resulted in a 45 % higher f_{R3}/f_{R1} ratio compared to the control (SWSS). PPS and BF, conversely, exhibited a decrease in f_{R3}/f_{R1} and a shift towards brittle behavior. Micro-fiber hybridization of BF with either PPS or PVA fibers significantly enhanced f_{R3}/f_{R1} and promoted ductile behavior. Micro- and macro-fiber hybridization significantly enhanced ductility compared to mono micro-fibers, as evidenced by the increased f_{R3}/f_{R1} ratio. Hybrids 0.66PPL/0.33PVA and 0.66PPL/0.33BF increased f_{R3}/f_{R1} by 114 % and 466 % over PVA and BF, respectively. Notably, 0.66TPPL/0.33BF achieved the most significant improvement, surpassing both mono TPPL and BF by 24 % and 679 %, respectively. This is attributed to enhanced bonding of TPPL fibers due to partial replacement with BF, leading to improved reinforcement of the TPPL surrounding concrete.

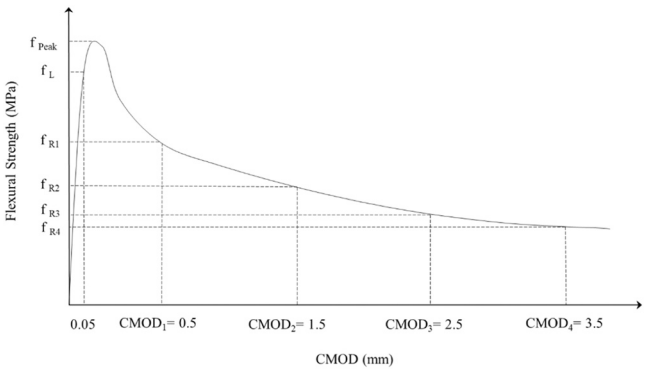

Fig. 15. Flexural behavior of FRC: Nominal stress vs. CMOD.

Micro-fiber hybridization significantly enhanced the f_{R1}/f_L ratio compared to mono fibers in all hybrid mixtures. Among these, the 0.66PPS/0.33PVA hybrid achieved the most pronounced improvement by about 244 % and 80 % over mono-PPS and -PVA, respectively. Micro/macro fiber hybridization significantly improved f_{R1}/f_L compared to micro-fibers alone, but negatively impacted compared to mono macro-fibers. Notably, only the PPL fiber achieved $f_{R1}/f_L > 0.4$ and $f_{R3}/f_{R1} > 0.5$, demonstrating adequate reinforcement in SWSSC. While hybridization offers potential, a higher total dosage is needed to meet reinforcement substitution requirements.

4. Synergistic effects of fiber hybridization

Synergistic effects of various fibers in hybrid system determine hybridization success. This study employed the synergistic coefficient (SC) to evaluate the fracture performance of these combinations relative to single fibers. The SC was calculated using Eq. (13) [37, 76] at a constant fiber volume fraction (V_f) of 0.25 %. A positive value indicates improved performance relative to the individual fibers.

$$SC = \frac{R_{hybrid,a+b}^{(V_f)} - \max\left(R_{mono,a}^{(V_f)}, R_{mono,b}^{(V_f)}\right)}{\max\left(R_{mono,a}^{(V_f)}, R_{mono,b}^{(V_f)}\right)} \tag{13}$$

where $R_{hybrid,a+b}$ is the fracture toughness properties—flexural strength, fracture energy and two fracture parameters (K_{IC}^{ini}, and K_{IC}^{un})— of hybrid FR-SWSSC, $R_{mono,a}$ and $R_{mono,b}$ are the fracture properties of mono-fibers, respectively.

The synergistic coefficients in Fig. 18 indicate that the incorporation of fibers in all hybrid systems resulted in a significant increase in the K_{IC}^{ini} and showed positive synergy. However, the specific fiber type and dosage are critical factors influencing the positive synergy observed for ultimate fracture toughness (K_{IC}^{un}). Hybridizing 0.33PPS/0.66BF and 0.66PPS/0.33BF fibers exhibited positive synergy in all fracture toughness parameters compared to mono-fibers. PPS/BF and PPS/PVA hybrids exhibited enhanced G_F and positive synergy, likely due to PVA and BF improving bonding strength and PPS fibers enhancing elongation, ultimately leading to increased fracture energy. Incorporation of PPL fibers with BF, PPS, and PVA generally resulted in decreased G_F and flexural strength. However, the 0.33PPL/0.66BF combination exhibited a synergistic enhancement in flexural strength. This positive synergy was attributed to the ability of BF to improve the bonding strength of PPL fibers with concrete matrix. Conversely, increasing BF content within the hybrid system led to heightened brittleness due to BF corrosion in SWSSC, resulting in a negative synergistic effect on energy dissipation. Furthermore, the influence of PPL fiber content on the energy dissipation mechanisms within the PPL/micro-fiber hybrid system was pronounced. TPPL hybridization with PVA or BF resulted in positive synergy for flexural strength, likely due to the superior flexibility and distribution of TPPL fibers compared to PPL, leading to improved synergy within the hybrid system. Notably, only the 0.66TPPL/0.33PVA combination displayed positive synergy for G_F, possibly due to the superior bonding strength of PVA fibers compared to BF. This stronger bonding reinforced the surrounding concrete matrix of TPPL, promoting fiber rupture and enhancing energy dissipation. Additionally, TPPL/BF hybridization exhibited positive synergy for K_{IC}^{un}, whereas TPPL/PVA displayed a negative effect.

Synergistic coefficient analysis revealed that fiber addition differentially impacted properties. Selecting the optimal fiber type or mix based on maximized overall fracture performance was therefore critical. To achieve this, the combined mechanical performance (CMP) of all mixes, calculated using Eq. (14) [68], was compared to plain SWSSC. A

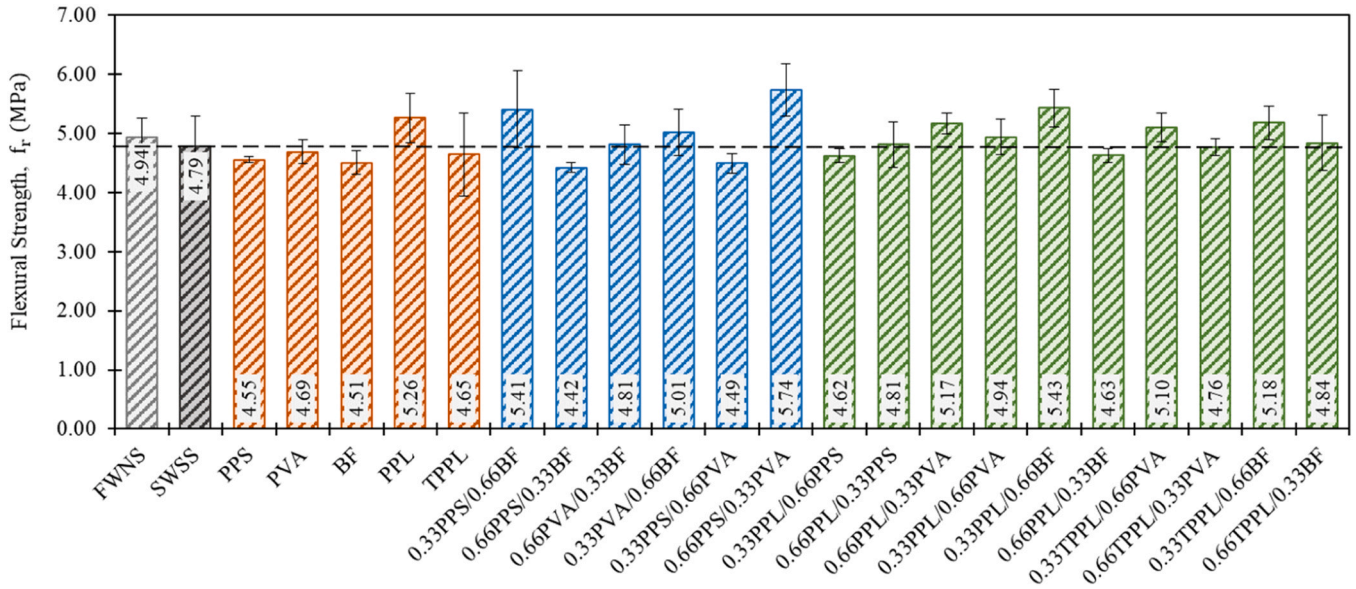

Fig. 16. The peak flexural strength of FR-SWSSC.

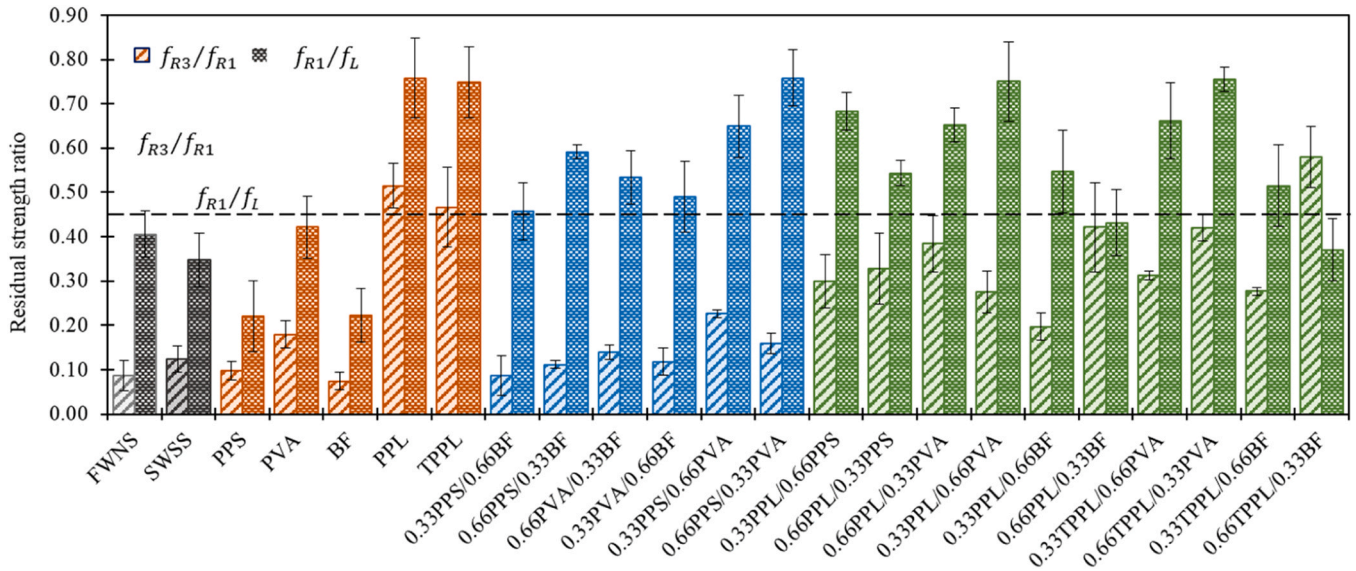

Fig. 17. The post-peak residual flexural strength of FR-SWSSC.

CMP exceeding 1.0 indicated superior overall fracture behavior. This study assigned equal weight to all fracture parameters, neglecting their individual significance.

$$CMP = \frac{1}{4} \times \left(\frac{f_{r,fiber}}{f_{r,SWSS}} + \frac{G_{F,fiber}}{G_{F,SWSS}} + \frac{K^{ini}_{IC,fiber}}{K^{ini}_{IC,SWSS}} + \frac{K^{un}_{IC,fiber}}{K^{un}_{IC,SWSS}} \right) \tag{14}$$

The results of the *CMP* study for FR-SWSSC mixes were compared with those of plain SWSSC and are illustrated in Fig. 19. The results showed that PPS and BF fibers had the lowest *CMP* value, while mono PPL and TPPL mixtures had the highest. The enhanced CMP of PPL fibers can be attributed to their higher volume fraction when utilized in a mono configuration. Experimental findings demonstrated that the PPL fiber content within the hybrid system significantly influenced its synergistic interaction with micro-fibers. As such, augmenting the PPL fiber dosage in the hybrid system, in conjunction with the complementary effects of PVA and BF micro-fibers, could potentially result in superior fracture behavior. This potential enhancement was ascribed to the high chemical bond established between the PVA and BF micro-fibers and the concrete matrix. CMP results indicated that PPL fibers outperformed PPS fibers, despite sharing a common base material. The superior CMP value of PPL (1.45 vs. 0.85 for PPS) facilitated enhanced crack bridging and energy dissipation due to its greater length. Moreover, the rough surface of PPL fibers promoted improved bonding with the concrete matrix, resulting in enhanced load transfer and fracture toughness. The combination of the factors including greater length, rough surface, and higher stiffness contributed to significantly higher fracture toughness of PPL fibers compared to PPS. Also, it was found that hybrid micro-fiber mixes had a *CMP* value greater than 1.0, except for 0.66PPS/0.33BF mixture. 0.66PPS/0.33PVA exhibited the greatest *CMP* value among micro-fiber hybrids. Among all micro and macro fiber hybridizations, hybrid PPL/PVA and TPPL/PVA resulted in the highest *CMP* value.

5. Conclusion

This study investigated the influence of hybrid fibers on fracture

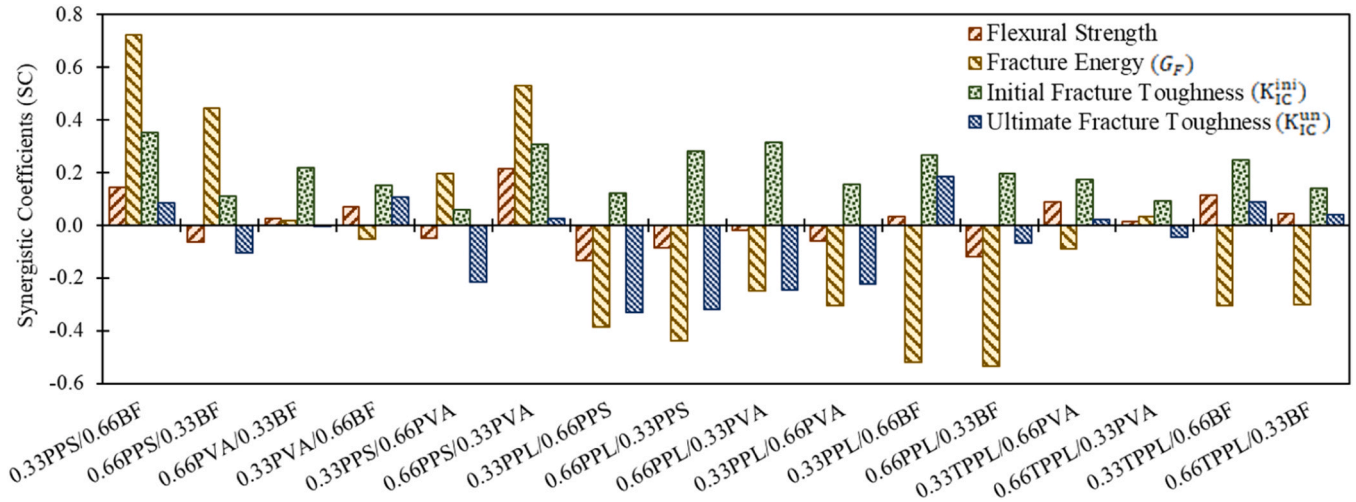

Fig. 18. Synergistic coefficients derived from fracture parameters of hybrid FR-SWSSC.

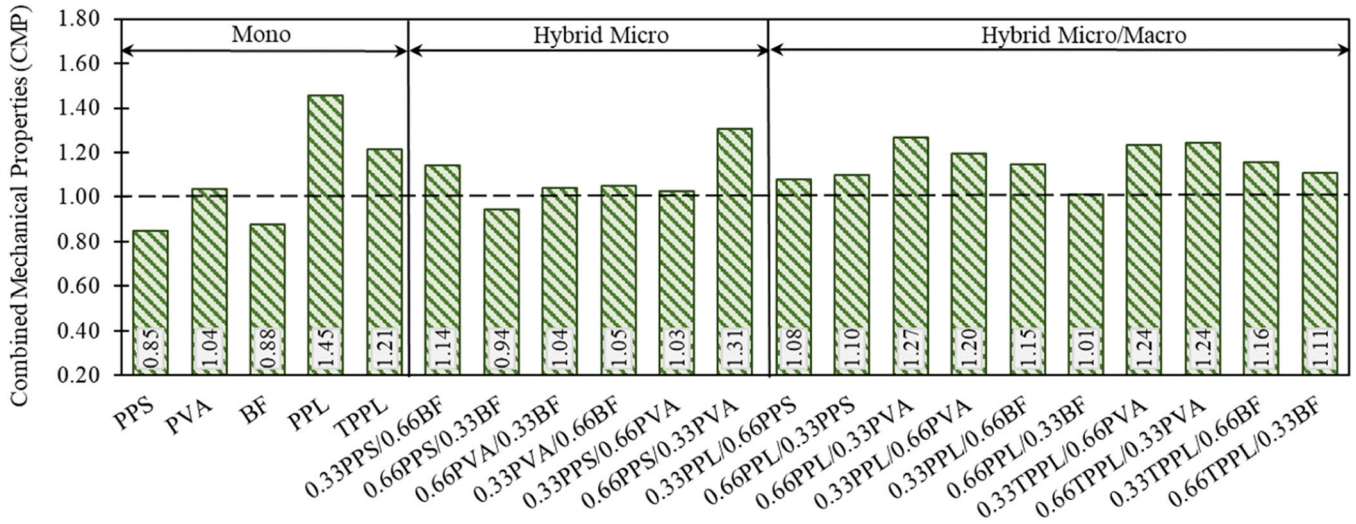

Fig. 19. The combined mechanical performance (CMP) of FR-SWSSC.

properties of fiber-reinforced seawater sea-sand concrete. Five fiber types were incorporated: micro-polypropylene (PPS), polyvinyl alcohol (PVA), and basalt (BF) alongside macro-polypropylene (PPL) and twisted polypropylene (TPPL), all at 0.25 % volume fraction. These were added to plain SWSSC in mono, hybrid micro, and hybrid micro-macro combinations to assess the hybridization effect. The findings offer valuable insights into how hybrid fibers can improve the fracture resistance of FR-SWSSC. Key results are presented below:

- Macro-fiber incorporation (PPL and TPPL) significantly improved the post-peak behavior of SWSSC. PPL and TPPL fibers increased fracture energy by 144 % and 93 %, respectively compared to the plain SWSSC at CMOD 3.5 mm. The enhanced performance was attributed to the length of macro-fibers, which effectively bridged macro-cracks at post-peak stages due to superior mechanical bonding strength.
- Micro-fiber inclusion in SWSSC marginally affected post-crack behavior, but hybridization significantly enhanced fracture performance. Hybridizing PPS with BF or PVA increased fracture energy at CMOD 3.5 mm by 176 % and 290 %, respectively, compared to mono PPS. This improvement likely stemmed from the weak bonding strength of PPS fibers, which PVA and BF effectively addressed, and their synergistic action in mitigating micro-cracks.
- Hybridizing PPL fibers with PPS, PVA, or BF significantly increased fracture energy at a CMOD of 3.5 mm compared to mono micro-fibers by 244 %, 66 %, and 68 %, respectively. Similarly, TPPL hybridization with PVA or BF enhanced fracture energy by 80 % and 93 %, respectively. The ability of PPL and TPPL fibers to bridge macro-cracks activated micro-fibers for synergistic behavior. Additionally, the strong chemical bonding of PVA and BF effectively reinforced the surrounding concrete matrix and improved macro-fiber bonding.
- The fracture process zone length (Δa_C) of SWSSC significantly increased with PVA, BF, PPL, and TPPL fibers, enhancing it by about 30, 19, 39, and 21 times, respectively. Fiber inclusion significantly enhanced cohesion toughness (K_{IC}^{C}), with PVA and PPL fibers yielding the most improvements, by about 54 and 93 times, respectively. This can be attributed to fiber bridging of micro-cracks, distributing tensile stress, and engaging a larger section compared to plain SWSSC, resulting in higher Δa_C and K_{IC}^{C}.
- Fiber hybridization significantly improved initial fracture toughness (K_{IC}^{ini}). The 0.66PVA/0.33BF combination exhibited the greatest enhancement in micro-fiber hybrids, surpassing both BF and PVA by 22 % and 17 %, respectively. This was attributed to the synergy of PVA/BF in SWSSC, enhancing matrix bonding and promoting

reinforcement efficiency. 0.66PPL/0.33PVA hybridization increased K_{IC}^{ini} by 25 % and 32 % relative to mono PVA and PPL, respectively. This synergy between the fibers resulted in enhanced bonding strength and concrete reinforcement, allowing PPL fibers to better resist crack initiation.

The study revealed that fiber hybridization in SWSSC showed promise for enhancing its fracture properties. Synergistic effects enhanced fracture performance compared to mono-fiber configurations, making it a promising material for coastal and offshore structures. Further research is needed to understand the behavior and optimize fiber content of hybrid FR-SWSSC under varying conditions. Additionally, long-term performance and durability in marine environments require evaluation. Overall, hybrid fibers offer significant potential for more resilient SWSSC structures.

CRediT authorship contribution statement

Allan Manalo: Writing – review & editing, Supervision. **Christopher Chow:** Writing – review & editing, Supervision. **Milad Bazli:** Writing – review & editing, Supervision. **Yan Zhuge:** Writing – review & editing, Supervision. **Xing Ma:** Writing – review & editing, Supervision. **Amirhesam Mashayekhi:** Writing – original draft, Investigation, Formal analysis, Data curation, Conceptualization. **Reza Hassanli:** Writing – review & editing, Supervision, Project administration, Methodology, Investigation, Conceptualization.

Declaration of Competing Interest

The authors declare that they have no known competing financial interests or personal relationships that could have appeared to influence the work reported in this paper.

Data Availability

Data will be made available on request.

Acknowledgements

The authors gratefully acknowledge the financial and laboratory support provided by the University of South Australia. We thank the technicians of the university's concrete laboratory for their assistance. We extend our appreciation to Adelaide Brighton Cement Ltd and Independent Cement and Lime Pty Ltd for donating OPC and GGBS, respectively, and to TEXO company for donating PPS and TPPL fibers. We are also grateful to Mr. Adam Bromley for his support. Additionally, we acknowledge the instruments and expertise of Microscopy Australia at the Future Industries Institute (FII), University of South Australia.

References

[1] S.A. Miller, A. Horvath, P.J. Monteiro, Impacts of booming concrete production on water resources worldwide, Nat. Sustain. 1 (1) (2018) 69–76.
[2] Y. Li, W. Liu, T. Mi, X. Ding, L. Tang, F. Xing, Durability study of seawater and sea-sand concrete under the combined effects of carbonation and chloride redistribution, J. Build. Eng. (2024) 109294.
[3] Slowey, K., Report: Global Construction Waste Will Almost Double by 2025. Construction Dive, 2018.
[4] Interior, U.S.G.S.Dd, Mineral commodity summaries 2020. 06.02. 2020, Reston, VA; https://pubs. er. usgs. gov/publication/mcs2020, 2020.
[5] A. Gholampour, T. Ozbakkaloglu, T.D. Ngo, Development of a waste-based eco-friendly structural mortar without Portland cement and natural sand. Struct. Concr. 22 (2021). E488-E500.
[6] Y. Li, C. Qiao, W. Ni, Green concrete with ground granulated blast-furnace slag activated by desulfurization gypsum and electric arc furnace reducing slag, J. Clean. Prod. 269 (2020) 122212.
[7] N. Gupta, R. Siddique, R. Belarbi, Sustainable and greener self-compacting concrete incorporating industrial by-products: a review, J. Clean. Prod. 284 (2021) 124803.
[8] J. Xiao, C. Qiang, A. Nanni, K. Zhang, Use of sea-sand and seawater in concrete construction: current status and future opportunities, Constr. Build. Mater. 155 (2017) 1101–1111.
[9] T. Dhondy, A. Remennikov, M.N. Shiekh, Benefits of using sea sand and seawater in concrete: a comprehensive review, Aust. J. Struct. Eng. 20 (4) (2019) 280–289.
[10] P. Li, W. Li, Z. Sun, L. Shen, D. Sheng, Development of sustainable concrete incorporating seawater: a critical review on cement hydration, microstructure and mechanical strength, Cem. Concr. Compos. 121 (2021) 104100.
[11] M. Etxeberria, J.M. Fernandez, J. Limeira, Secondary aggregates and seawater employment for sustainable concrete dyke blocks production: case study, Constr. Build. Mater. 113 (2016) 586–595.
[12] A. Younis, U. Ebead, P. Suraneni, A. Nanni, Fresh and hardened properties of seawater-mixed concrete, Constr. Build. Mater. 190 (2018) 276–286.
[13] M.Z.Y. Ting, K.S. Wong, M.E. Rahman, M. Selowara Joo, Mechanical and durability performance of marine sand and seawater concrete incorporating silicomanganese slag as coarse aggregate. Constr. Build. Mater. 254 (2020) 119195.
[14] P. Sikora, K. Cendrowski, M. Abd Elrahman, S.-Y. Chung, E. Mijowska, D. Stephan, The effects of seawater on the hydration, microstructure and strength development of Portland cement pastes incorporating colloidal silica, Appl. Nanosci. 10 (8) (2020) 2627–2638.
[15] Z. Shi, Z. Shui, Q. Li, H. Geng, Combined effect of metakaolin and sea water on performance and microstructures of concrete, Constr. Build. Mater. 74 (2015) 57–64.
[16] P. Li, W. Li, T. Yu, F. Qu, V.W.Y. Tam, Investigation on early-age hydration, mechanical properties and microstructure of seawater sea sand cement mortar, Constr. Build. Mater. 249 (2020) 118776.
[17] D. Vafaei, R. Hassanli, X. Ma, J. Duan, Y. Zhuge, Sorptivity and mechanical properties of fiber-reinforced concrete made with seawater and dredged sea-sand, Constr. Build. Mater. 270 (2021) 121436.
[18] M. Etxeberria, A. Gonzalez-Corominas, P. Pardo, Influence of seawater and blast furnace cement employment on recycled aggregate concretes' properties, Constr. Build. Mater. 115 (2016) 496–505.
[19] W. Lv, Z. Sun, Z. Su, Study of seawater mixed one-part alkali activated GGBFS-fly ash, Cem. Concr. Compos. 106 (2020) 103484.
[20] W. Liu, Y. Li, L. Tang, F. Xing, Modelling analysis of chloride redistribution in sea-sand concrete exposed to atmospheric environment, Constr. Build. Mater. 274 (2021) 121962.
[21] D. Vafaei, X. Ma, R. Hassanli, J. Duan, Y. Zhuge, Microstructural behaviour and shrinkage properties of high-strength fiber-reinforced seawater sea-sand concrete, Constr. Build. Mater. 320 (2022) 126222.
[22] J. Ahmad, R.A. González-Lezcano, A. Majdi, N. Ben Kahla, A.F. Deifalla, M.A. El-Shorbagy, Glass fibers reinforced concrete: overview on mechanical, durability and microstructure analysis, Materials 15 (15) (2022) 5111.
[23] Y. Li, J. Zhang, Y. He, G. Huang, J. Li, Z. Niu, B. Gao, A review on durability of basalt fiber reinforced concrete, Compos. Sci. Technol. 225 (2022) 109519.
[24] F. Ameri, J. de Brito, M. Madhkhan, R.A. Taheri, Steel fibre-reinforced high-strength concrete incorporating copper slag: mechanical, gamma-ray shielding, impact resistance, and microstructural characteristics, J. Build. Eng. 29 (2020) 101118.
[25] A. Gholampour, R. Hassanli, J.E. Mills, T. Vincent, M. Kunieda, Experimental investigation of the performance of concrete columns strengthened with fiber reinforced concrete jacket, Constr. Build. Mater. 194 (2019) 51–61.
[26] J.-X. Lin, Y. Song, Z.-H. Xie, Y.-C. Guo, B. Yuan, J.-J. Zeng, X. Wei, Static and dynamic mechanical behavior of engineered cementitious composites with PP and PVA fibers, J. Build. Eng. 29 (2020) 101097.
[27] N. Prasad, G. Murali, Exploring the impact performance of functionally-graded preplaced aggregate concrete incorporating steel and polypropylene fibres, J. Build. Eng. 35 (2021) 102077.
[28] J. Feng, Y. Su, C. Qian, Coupled effect of PP fiber, PVA fiber and bacteria on self-healing efficiency of early-age cracks in concrete, Constr. Build. Mater. 228 (2019) 116810.
[29] Y. Ling, P. Zhang, J. Wang, Y. Chen, Effect of PVA fiber on mechanical properties of cementitious composite with and without nano-SiO2, Constr. Build. Mater. 229 (2019) 117068.
[30] D. Vafaei, R. Hassanli, X. Ma, J. Duan, Y. Zhuge, Fracture toughness and impact resistance of fiber-reinforced seawater sea-sand concrete, J. Mater. Civ. Eng. 34 (5) (2022) 04022038.
[31] A. Mashayekhi, R. Hassanli, Y. Zhuge, X. Ma, C.W. Chow, Synergistic effects of fiber hybridization on the mechanical performance of seawater sea-sand concrete, Constr. Build. Mater. 416 (2024) 135087.
[32] Z. Yang, F. Lu, X. Zhan, H. Zhu, B. Zhang, Z. Chen, H. Zhang, Mechanical properties and mesoscopic damage characteristics of basalt fibre-reinforced seawater sea-sand slag-based geopolymer concrete, J. Build. Eng. 84 (2024) 108688.
[33] J. Kaidi, W. Xin, D. Lining, C. Zhiyuan, H. Huang, L. Xia, L. Jianxun, W. Zhishen, Mechanical properties of multi-scale mono/hybrid non-metallic fiber-reinforced ultra-high performance seawater sea-sand concrete, Constr. Build. Mater. 401 (2023) 132922.
[34] Z. Chenggong, W. Zhiyuan, Z. Zhenyu, G. Qiuyu, W. Xinrui, Z. Renda, Research on different types of fiber reinforced concrete in recent years: an overview, Constr. Build. Mater. 365 (2023) 130075.
[35] S.F.U. Ahmed, H. Mihashi, Strain hardening behavior of lightweight hybrid polyvinyl alcohol (PVA) fiber reinforced cement composites, Mater. Struct. 44 (6) (2011) 1179–1191.
[36] Ö. Şükrü, Ç. Ömer, The hybrid effects of basalt and PVA fiber on properties of a cementitious composite: physical properties and non-destructive tests, Constr. Build. Mater. 312 (2021) 125292.

[37] D.-L. Nguyen, D.-K. Thai, M.N.-T. Lam, Synergy in flexure of high-performance fiber-reinforced concrete with hybrid steel fibers, J. Mater. Civ. Eng. 34 (6) (2022) 04022090.
[38] K. Mehran, C. Mingli, X. Chaopeng, A. Majid, Effectiveness of hybrid steel-basalt fiber reinforced concrete under compression, Case Stud. Constr. Mater. 16 (2022) e00941.
[39] Y.M. Abbas, L.A. Hussain, M.I. Khan, Constitutive compressive stress–strain behavior of hybrid steel-PVA high-performance fiber-reinforced concrete, J. Mater. Civ. Eng. 34 (1) (2022) 04021401.
[40] C. Kai, X. Lihua, T. Tao, H. Le, L. Jian, H. Jian, L. Huan, C. Yin, Mechanical behavior of multiscale hybrid fiber reinforced recycled aggregate concrete subject to uniaxial compression, J. Build. Eng. 71 (2023) 106504.
[41] A.H. Abdel-Karim, G.I. Khalil, A.E. Ewis, M.H. Makhlouf, Impact of developed hybrid polypropylene fiber inclusion on the flexural performance of concrete beams reinforced with innovative hybrid bars, Constr. Build. Mater. 409 (2023) 134113.
[42] Z. Çelik, A.F. Bingöl, Fracture properties and impact resistance of self-compacting fiber reinforced concrete (SCFRC), Mater. Struct. 53 (3) (2020) 1–16.
[43] H. Pakravan, M. Jamshidi, M. Latifi, The effect of hydrophilic (polyvinyl alcohol) fiber content on the flexural behavior of engineered cementitious composites (ECC), J. Text. Inst. 109 (1) (2018) 79–84.
[44] J. Ríos, H. Cifuentes, C. Leiva, M. Ariza, M. Ortiz, Effect of polypropylene fibers on the fracture behavior of heated ultra-high performance concrete, Int. J. Fract. 223 (1) (2020) 173–187.
[45] H.R. Pakravan, M. Latifi, M. Jamshidi, Hybrid short fiber reinforcement system in concrete: a review, Constr. Build. Mater. 142 (2017) 280–294.
[46] Z. Yang, X. Zhan, H. Zhu, B. Zhang, R. Li, Z. Dong, H.W. Kua, Eco-sustainable design of seawater sea-sand slag-based geopolymer mortars incorporating ternary solid waste, Constr. Build. Mater. 431 (2024) 136512.
[47] S. Yang, C. Zang, J. Xu, G. Fan, Determination of fracture parameters of seawater sea sand concrete based on maximum fracture load, J. Mater. Civ. Eng. 32 (1) (2020) 04019315.
[48] K.P. Fattah, A.K. Al-Tamimi, W. Hamweyah, F. Iqbal, Evaluation of sustainable concrete produced with desalinated reject brine, Int. J. Sustain. Built Environ. 6 (1) (2017) 183–190.
[49] Z.H. Zhang, Z.Q. Sang, L.Y. Zhang, Z.X. Ma, Y. Zhang, Experimental research on durability of concrete made by seawater and sea-sand, Adv. Mater. Res. (2013) (Trans Tech Publ).
[50] Y. Zheng, Y. Zhang, J. Zhuo, Y. Zhang, C. Wan, A review of the mechanical properties and durability of basalt fiber-reinforced concrete, Constr. Build. Mater. 359 (2022) 129360.
[51] H. Dou, J. Bai, H. Lu, T. Zhang, L. Kong, Z. Bai, W. Li, Effect of TiO2 on preparation condition, mechanical properties and alkali resistance of continuous basalt fibers, Cem. Concr. Compos. 136 (2023) 104861.
[52] Australia, S., Methods of testing concrete-Preparation of concrete mixes in the laboratory. 1994, AS.
[53] R.H. Faraj, A.F.H. Sherwani, A. Daraei, Mechanical, fracture and durability properties of self-compacting high strength concrete containing recycled polypropylene plastic particles, J. Build. Eng. 25 (2019) 100808.
[54] J.-c Zhang, B.-j Li, W.-y Chen, R.-x Guo, Experimental investigations on tensile strength and fracture toughness of a polyoxymethylene fiber reinforced concrete, Theor. Appl. Fract. Mech. 130 (2024) 104250.
[55] F. Mukhtar, Simulation of fracture behavior in seawater and sea-sand mixed recycled coarse aggregate concrete under three-point bending, Theor. Appl. Fract. Mech. 131 (2024) 104413.
[56] N. Amin, S. Bijan, V. Kirk, Effect of polyvinyl alcohol (PVA) fibre on dynamic and material properties of fibre reinforced concrete, Constr. Build. Mater. 49 (2013) 374–383.
[57] Standard, J., Method of Test for Fracture Energy of Concrete by Use of Notched Beam. JCI-S-001e2003, Japan Concrete Institute, 2003.
[58] C. Xie, M. Cao, M. Khan, H. Yin, J. Guan, Review on different testing methods and factors affecting fracture properties of fiber reinforced cementitious composites, Constr. Build. Mater. 273 (2021) 121766.
[59] M.A. Rasheed, S.S. Prakash, G. Raju, Y. Kawasaki, Fracture studies on synthetic fiber reinforced cellular concrete using acoustic emission technique, Constr. Build. Mater. 169 (2018) 100–112.
[60] F. Kazemian, H. Rooholamini, A. Hassani, Mechanical and fracture properties of concrete containing treated and untreated recycled concrete aggregates, Constr. Build. Mater. 209 (2019) 690–700.
[61] P. Zhang, P. Yuan, J. Guan, J. Guo, Fracture behavior of multi-scale nano-SiO2 and polyvinyl alcohol fiber reinforced cementitious composites under the complex environments, Theor. Appl. Fract. Mech. 122 (2022) 103584.
[62] S. Xu, H.W. Reinhardt, A simplified method for determining double-K fracture parameters for three-point bending tests, Int. J. Fract. 104 (2000) 181–209.
[63] S. Xu, H.W. Reinhardt, Determination of double-K criterion for crack propagation in quasi-brittle fracture, Part I: experimental investigation of crack propagation, Int. J. Fract. 98 (2) (1999) 111–149.
[64] S. Xu, H.W. Reinhardt, Determination of double-K criterion for crack propagation in quasi-brittle fracture, Part II: analytical evaluating and practical measuring methods for three-point bending notched beams, Int. J. Fract. 98 (1999) 151–177.
[65] S.P. Shah, Size-effect method for determining fracture energy and process zone size of concrete, Mater. Struct. 23 (1990) 461–465.
[66] Hiroshi, T., P. Paris, and G. Irwin, The Stress Analysis of Cracks Handbook. ASME, New York, 2000.
[67] J. Wang, E. Liu, L. Li, Multiscale investigations on hydration mechanisms in seawater OPC paste, Constr. Build. Mater. 191 (2018) 891–903.
[68] M. Li, D. Xing, Q.-B. Zheng, H. Li, B. Hao, P.-C. Ma, Variation on the morphology and tensile strength of basalt fiber processed in alkali solutions, Constr. Build. Mater. 335 (2022) 127512.
[69] Q. Wang, Y. Ding, N. Randl, Investigation on the alkali resistance of basalt fiber and its textile in different alkaline environments, Constr. Build. Mater. 272 (2021) 121670.
[70] P. Zhang, Y. Yang, J. Wang, M. Jiao, Y. Ling, Fracture models and effect of fibers on fracture properties of cementitious composites—a review, Materials 13 (23) (2020) 5495.
[71] Z. Çelik, A.F. Bingöl, Fracture properties and impact resistance of self-compacting fiber reinforced concrete (SCFRC), Mater. Struct. 53 (2020) 1–16.
[72] M. Code, fib model Code for concrete structures, Struct. Concr. (2010) 14.
[73] Institution, B.S., Test Method for Metallic Fibre Concrete: Measuring the Flexural Tensile Strength (limit of Proportionality (LOP), Residual). 2008: BSI.
[74] R. TC162-TDF, Test and design methods for steel fibre reinforced concrete, Mater. Struct. 36 (2003) 560–567.
[75] M. Di Prisco, G. Plizzari, L. Vandewalle, Fibre reinforced concrete: new design perspectives, Mater. Struct. 42 (2009) 1261–1281.
[76] P.T. Hoan, N.T. Thuong, Shear resistance of ultra-high-performance concrete reinforced with hybrid steel fiber subjected to impact loading, J. Sci. Technol. Civ. Eng. (STCE)-HUCE 13 (1) (2019) 12–20.